

## 6 Introduction

The problem of sound wave scattering by elastic objects has been under investigation for several decades, as an effective solution to the problem is needed in various scientific and engineering areas. For example, this problem appears in naval operations where methods of efficient and reliable target detection are of major importance.

Apart from military applications, scattering techniques may be used in many civil areas of science and engineering. For example, the fishing industry uses scattering devices to detect and control fish shoals, environmental scientists use sonar scanning for monitoring parameters of the ocean environment like salinity, ocean vortices, icebergs etc. Methods similar to ocean sonar techniques exist also in the mining industry, where it is possible to detect mineral deposits by recording and investigating scattered seismic waves.

Methods developed in acoustic scattering also may be applied to the scattering of electromagnetic waves where the governing equations and boundary conditions are similar. This fact potentially opens large areas of application in atmospheric science and radar technology.

However, despite the abundance of the literature on the subject of scattering, quickly converging and numerically effective solutions still are not available for acoustic scattering by elastic objects in waveguides. Scattering in waveguides is very complicated due to presence of waveguide boundaries, which cause multiple reflection of acoustic waves. In the ocean, anisotropy of the waveguide, uneven bottom, and surface waves make the problem even more complicated (Fig. 1). The elasticity of scattering objects, where they can not be considered as absolutely rigid or soft, adds further complication.

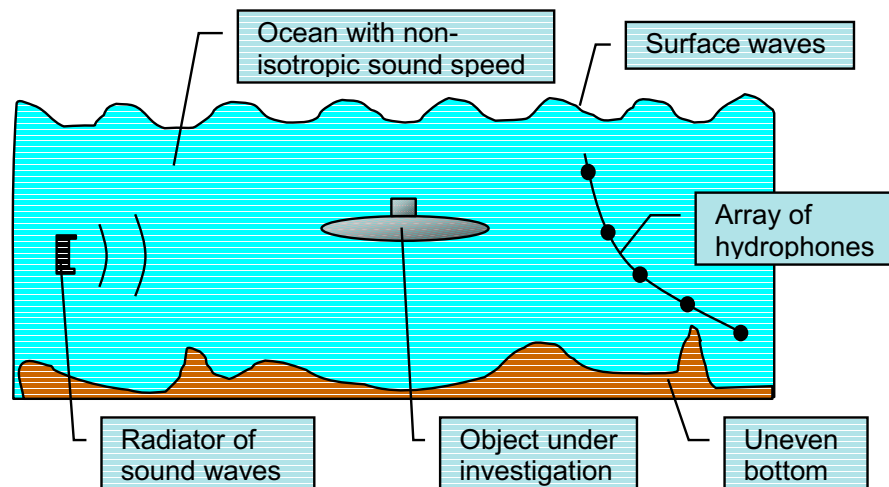


Figure 1. The scattering problem in ocean.

The present work suggests a novel approach to the scattering of waves in waveguides. This approach gives a quickly converging and

numerically efficient solution to the problem. It provides the possibility of calculating the amplitudes of the reflected acoustic field as well as the parameters of the scattering process in waveguides quickly and with high accuracy. The method differs from existing methods by providing a solution, which takes into account all the waveguide modes up to infinite order.

The power of the new method is demonstrated by its application to the problem of 2-dimensional scattering by cylindrical objects in a shallow waveguide. One of the cases considered is scattering by homogeneous cylinders (including multiple cylinders located close to each other), and the second case is scattering by an air filled cylindrical elastic shell.

For these two cases, various characteristics are obtained. These characteristics allow important physical conclusions to be made about the influence of the parameters of the system waveguide/scattering object on parameters of the scattered acoustic wave and oscillations of the object itself. One of the most significant conclusions is the recognition of the importance of the higher-order waveguide modes. Their inclusion is essential for the correct calculations of the signal in the far field.

## 7 Literature Review

### 7.1 Introduction

Waves along the boundary of an elastic medium have been under investigation since the late 19<sup>th</sup> century, when Lord Rayleigh (1885) provided a mathematical solution for waves on the surface of an elastic body which later were named after him. In the second half of the 20<sup>th</sup> century, however, the following was observed: it was found that oscillations and waves occurring in the near field may strongly influence the characteristics of the scattering process in the far field. It also was found, that waves of various types may exist near curved surfaces of elastic scattering objects, producing effects like multiple acoustic echoes. This fact stimulated the interest of many researchers in the influence of surface waves near scattering objects on the parameters of the scattered signal in the far field.

### 7.2 Circumferential waves around solid cylinders and spheres.

Various researchers have investigated the subject since the early 1960s when multiple responses in the scattered acoustic signal to a single pulse incident wave were reported (Barnard and McKinney, 1961). It has been postulated that the existence of circumferential waves on the surface of the cylinder accounts for the observed echo structure (Horton *et al*, 1962). Four main types of circumferential waves, which propagate near the surface of elastic solid scattering objects, have been identified: Rayleigh, Stoneley, Franz, and Whispering Gallery (WG) types of waves.

Early theoretical works on the subject were restricted to the limit of cylinders large in comparison with the acoustic wavelength. Grace and Goodman (1966) theoretically obtained approximate expressions for velocity and attenuation for waves travelling around a solid cylinder immersed in water. They found that such waves without an incident acoustic field could exist at two values of the acoustic wavenumber  $k$ , one real and one complex. These values were associated with two different types of circumferential waves propagating around the cylinder. The complex root corresponds to the Rayleigh wave, which radiates acoustic energy due to  $\text{Im}(k) > 0$ , and the real root describes the Stoneley wave, which radiates very inefficiently.

The Rayleigh and Stoneley waves have been known for many years (Rayleigh, 1885, Stoneley, 1924) and their description can be found, for example, in "Waves in Layered Media" by Brekhovskikh (1960). The Rayleigh wave propagates mostly in the solid material and its velocity  $c_r$  is close to the transversal wave velocity  $c_t$  in the solid. The mechanism of the Rayleigh wave is close to that of surface waves on water, where gravity plays the role of elastic forces. The Stoneley wave propagates mostly in the surrounding fluid and causes only small displacements in the elastic material of the scattering object.

The Stoneley wave velocity  $c_S$  is close to the sound speed in the fluid  $c$ . Rayleigh and Stoneley type waves in the limit of the large cylinder diameter were studied analytically by Lapin (1969). Frisk *et al* (1975) obtained dispersion and attenuation curves numerically for these types of surface waves.

Doolittle *et al* (1967, 1968) applied Sommerfeld-Watson Transformation (SWT) to the problem of diffraction of sound pulses on elastic cylinders. The SWT method allows the transformation of the complex  $k$  plane into the complex mode number  $\nu$  plane. It was reported that the Franz waves have much larger  $\text{Im}(\nu)$  than the Rayleigh waves, so they radiate more efficiently and are damped more quickly. The group velocities of the circumferential sound pulses were obtained. It was shown that Franz poles produce circumferential waves that enter and leave the cylinder surface tangentially, whereas the Rayleigh circumferential waves enter and leave at a critical angle. The existence of the Rayleigh waves on solid elastic cylinders was experimentally verified by Goodman *et al* (1967).

Rayleigh and Stoneley waves can exist on both plane and curved surfaces. There have been identified two more types of waves, which exist only near curved boundaries. The first of these was discovered by Franz (1952) in the scattering of electromagnetic waves. In fact, his “creeping waves” are just one of possible representations of the field near the scattering object. The near field was imagined as a series of circumferential waves, propagating around the object and “creeping” into the shadow region (Überall *et al*, 1966). This is the only type of circumferential waves, which propagates near absolutely rigid or soft objects, because elastic properties of the object do not play any significant role in the mechanism of the wave propagation. In the paper by Überall *et al*. (1966) velocities and attenuations of several Franz’s lower order modes were found theoretically for rigid and soft cylinders using the SWT.

The second type, vertically polarised Whispering Gallery (WG) modes, was theoretically described by Brekhovskikh (1967, 1968). He found that WG modes in the case of the vertical polarisation consist of longitudinal and transversal components, and the transversal displacement penetrates the elastic body much deeper than the longitudinal one. (Vertical polarisation means that the displacement vector lies in a plane normal to the boundary. Horizontal polarisation, where the displacement vector is parallel to the cylinder axis, was described by Rayleigh (1885)). The velocity  $c_{wg}$  of the vertically polarised Whispering Gallery modes lies between  $c_t$  and  $c_l$ .

Influence of circumferential waves on the acoustic signal scattered by elastic objects has been investigated in detail. Changes of the circumferential pulse shape in the case of absolutely soft cylinder were theoretically studied by McNicholas *et al* (1968) for both delta-function and finite-step-function initial pulse shapes. Comparison of

the theoretical predictions of the scattering of long acoustic pulses with experimental results was done by Numrich *et al* (1986). They showed that long-pulse scattering leads to a sequence of overlapping reflected and surface-wave pulses which give rise to several types of interference phenomena. The acoustic response of the cylinder at resonance was shown to synthesise an approximately exponentially decaying ringing response of a resonant normal mode. It was stated also that identifying the eigenvibrations of a submerged elastic target by the use of long acoustic pulses is a powerful tool for target identification.

Frisk and Überall (1976) established the connection between creeping waves on curved and flat surfaces. They showed that Whispering Gallery modes combine to form both longitudinal and transverse lateral waves on a flat surface; the cylindrical Rayleigh wave tends to the flat Rayleigh wave, while the Franz and Stoneley waves disappear. The same authors presented a study of the Whispering Gallery modes (Dickey *et al*, 1976), where they obtained dispersion curves and normalised attenuations for WG waves.

The physical nature of the creeping wave resonances was shown by Überall *et al* (1977). It was suggested that each resonance corresponds to the frequency at which one of the creeping wavelengths fits the body's circumference an integer number of times. Dickey and Überall (1978) showed the mechanism of resonance reinforcement of the elastic-type surface waves as a result of their repeated circumnavigations of the surface.

The introduction of Resonance Scattering Theory (RST) by Flax *et al* (1978) facilitated better understanding of creeping waves on the surface of an elastic scattering object. They demonstrated that the strongly fluctuating behaviour of the scattered signal is caused by a superposition of generally narrow resonances in the individual normal modes and a background of rigid- or soft-body scattering. They showed that for scattering at a frequency in between two eigenfrequencies of the elastic body, the scatterer appears as an impenetrable object. Conversely, at and near an eigenfrequency, a scattering resonance is excited by the incident wave. The resonance scattering interferes with background scattering, which causes the strongly oscillating structure in the total scattering amplitude.

The main properties of the different types of circumferential waves existing near the surface of a solid cylinder are shown in the Table 1. Radiation damping of the waves is determined by the normalised attenuation term  $\text{Im}(kR)/\text{Re}(kR)$ . This term has been used to calculate radiation damping for the lowest order mode for each type of wave using data published by Frisk *et al* (1975) and Numrich *et al* (1986).

**Table 1.**

*Types of circumferential waves on the surface of a solid cylinder and their properties.*

	<b>Rayleigh</b>	<b>Stoneley</b>	<b>Franz</b>	<b>Whispering Gallery</b>
<b>Where propagates</b>	Solid	Fluid	Fluid	Solid
<b>Exists on plane surface</b>	Yes	No	No	Tend to lateral waves
<b>Speed</b>	$c_r \sim c_t$	$c_s \leq c$	$c_f \leq c$	$c_b < c_{wg} < c_l$
<b>Exists near absolutely rigid body</b>	No	No	Yes	No
<b>Radiation Damping</b>	Average	Low	High	Low
<b>Im(ka)/Re(ka) for aluminium cylinder in water</b>	~0.05	~0.01	~0.1	<0.02
<b>Physical nature</b>	Similar to waves on the water surface	Acoustic wave in fluid propagating tangentially to elastic surface	Higher order modes in the fluid arising due to the curvature of the boundary	Multiple reflections of elastic waves from internal curved surface of elastic body

### **7.3 Circumferential waves around cylindrical and spherical shells.**

All of the above mentioned publications deal with circumferential surface waves near *solid* objects. It also was discovered that fluid-filled *shells* might have circumferential waves. Doolittle and Überall (1966) derived expressions for the scattering matrix coefficients in the case of scattering by a shell. Numerical investigation of the scattering by shells with the use of SWT, similar to the analysis done by Doolittle *et al* (1968) for the scattering by solid elastic cylinders, was carried out by Ugincius and Überall (1968). Existence of Rayleigh and Franz type waves in the scattering process by shells was confirmed. The influence of elastic reaction of a solid spherical shell in air on the resultant acoustic echoes was studied by Hickling (1967). He demonstrated numerically that a sequence of pulses in the reflected signal existed for all shell thicknesses due to the elastic resonances of the scattering shell. However, the effect was strongest for thin shells made of light material.

The Resonance Scattering Theory was applied to the scattering by fluid-filled elastic cylindrical shells in a liquid by Murphy *et al* (1978).

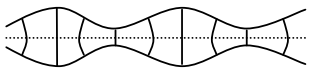
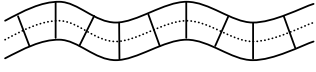
They showed that the background term, which must be subtracted to obtain resonances in the scattered signal, depends strongly on the shell thickness. For a thin shell, the background corresponds to a soft cylinder, while the background for a thick shell corresponds to the scattering from the rigid cylinder.

Investigation of the scattering by a shell using exact equations of elastodynamics was done by Gaunard and Brill (1984). They obtained a diagram showing the location of resonances of different types on the complex wavenumber plane. The diagram showed that Rayleigh waves have a different behaviour (larger radiation and damping) compared to the Whispering Gallery waves. Good agreement between the RST predictions and experimental results was achieved also by Izbicki *et al* (1986).

In addition to the circumferential waves described above, an elastic shell may carry waves of another type, Lamb waves, which are essentially normal modes of the layer of elastic material (Victorov, 1967). Their main properties and their spatial structure are shown in Table 2.

**Table 2.**

*Types of Lamb waves and their properties.*

	<b>Symmetric, <math>S_n</math></b>	<b>Asymmetric, <math>A_n</math></b>
<b>Where propagates</b>	Elastic layer	Elastic layer
<b>Speed (Victorov, 1967)</b>	$c_{ls} > c_t$	$c_{la} < c_t, n = 0$ $c_{la} > c_t, n > 0$
<b>Limit as the layer thickness increases (Talmant <i>et al</i>, 1988)</b>	Whispering Gallery wave	Rayleigh wave
<b>Spatial structure of zero-order mode (Victorov, 1967)</b>		

The existence of Lamb waves on a thin shell and their relationships with the other types of surface waves on a rigid cylinder was shown for cylindrical (Talmant *et al*, 1988) and spherical (Talmant *et al*, 1989) shells. As the shell thickness tends to zero, the first Whispering Gallery wave tends to the lowest symmetric Lamb wave, and the Rayleigh wave tends to the lowest asymmetric Lamb wave. Breitenbach *et al* (1983) also demonstrated that for thin shells transitions from Rayleigh-type surface waves to Lamb-type waves take place. A variety of resonance features in the back-scattering cross sections of an air-filled spherical shell submerged in water was studied by Gaunard and Werby (1991). They showed that air-borne

reverberations inside the shell would manifest themselves as a series of very narrow spikes.

Attention has been paid also to the *transmission* of sound waves through the interior of the elastic objects. Brill and Überall (1971) obtained expressions for wavefronts and arrival times for the acoustic waves transmitted through solid elastic cylinders at large frequencies ( $ka > 350$ ,  $a$  is the cylinder radius). It was stated that every ray which enters the cylinder is split into longitudinal and transverse components. Amplitudes of the transmitted waves were calculated.

A review of the literature devoted to Resonance Scattering Theory (RST) was done by Gaunaurd (1989). The review contains many results obtained by the use of the RST in acoustic and elastic scattering by homogeneous scattering objects such as spheres and cylinders. The applications of RST to various configurations are discussed. Validating experiments are described, and a bibliography containing 260 references and emphasising target-identification and target-camouflaging aspects of the RST is provided.

The above mentioned publications emphasise the importance of oscillations and waves within and near the scattering objects for determining characteristics of the scattering process in the far field. However, nearly all of them deal with the scattering in an unbounded fluid. Those articles which are devoted to scattering in waveguides consider only non-resonant phenomena, because of the complexity of the problem of the resonant scattering. Indeed, to calculate scattering by a resonant body in a waveguide, it is necessary to take into account multiple reflections of acoustic energy, radiated by the body, from the waveguide boundaries and the body itself. The current work suggests a new analytical and numerical method of solving such a problem and considers its applications to the scattering by a set of homogeneous elastic cylinders and by a gas-filled elastic cylindrical shell.



## 8 Theoretical foundations

### 8.1 Introduction

The theoretical basis of the MMI method was developed in articles by Belov *et al* (1994a, 1994b, 1994c, 1994d, 1998), Zinoviev and Belov (1998) for scattering by one and many homogeneous cylinders, and in articles by Zinoviev (1997, 2000) and Zinoviev and Bies (1998) for scattering by an air-filled cylindrical shell. This chapter contains an example of the application of the method to the case of sound scattering by a set of homogeneous cylinders with arbitrary boundary conditions on the waveguide walls (Belov *et al*, 1998).

### 8.2 Statement of the Problem

#### 8.2.1 Waveguide Layout

A planar two-dimensional waveguide is to be considered, which is filled with a perfect compressible fluid of density,  $\rho$ , sound speed,  $c$ ; and containing  $N$  localised inhomogeneities composed of round, elastic, infinite parallel cylinders, each of radius  $R_v$ , density  $\rho_v$ , and having Lamé coefficients  $\lambda_v, \mu_v$ , where  $v = 1, 2, \dots, N$ . A cross-section of the waveguide is shown in Fig.2. The waveguide is bounded above and below by parallel planes located at  $x = 0$  and  $x = D$ . The axes of the embedded cylinders are parallel to the  $z$ -axis of the waveguide and cross the  $z = 0$  plane at points  $(X_v, Y_v)$ . The analysis presented here is restricted to the two-dimensional steady-state problem with temporal dependence  $\exp(-i\omega t)$ .

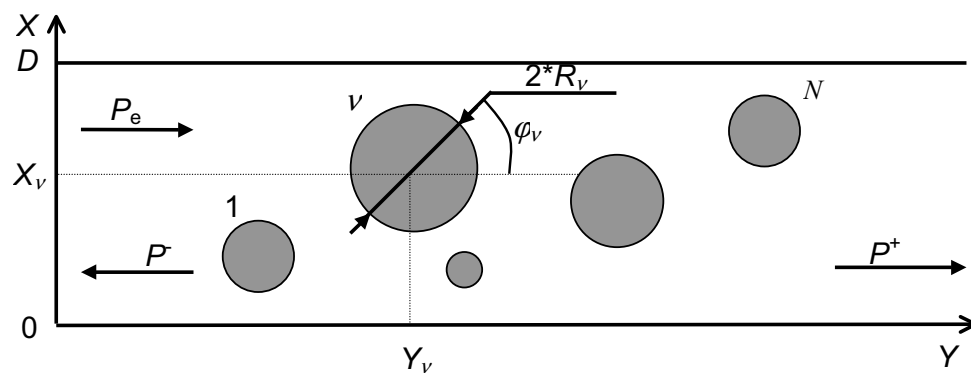


Figure 2. The layout of the waveguide with  $N$  cylinders.

## 8.2.2 Equations and Boundary Conditions

The acoustic field in the waveguide is described by a pressure field  $P(x, y)$  which is a sum of the incident wave  $P_e$  and waves  $P_{sv}$  scattered by the  $\nu$ -th cylinder:

$$P(x, y) = P_e(x, y) + \sum_{\nu=1}^N P_{sv}(x, y). \quad (1)$$

Elastic oscillations in each cylindrical body is described by the scalar potential,  $\Phi^{(\nu)}(r_\nu, \varphi_\nu)$ , and the  $z$ -component of the vector potential of displacements in an elastic body,  $F^{(\nu)}(r_\nu, \varphi_\nu)$ . The displacement vector in the cylinders is determined by:

$$\Delta \vec{r}_\nu(r_\nu, \varphi_\nu) = \nabla \Phi(r_\nu, \varphi_\nu) + \nabla \times F(r_\nu, \varphi_\nu), \quad (2)$$

where  $r$  and  $\varphi$  are polar coordinates with the origin in the centre of the cylinder, and  $z$  is the axial coordinate. The coordinates  $r_\nu$  and  $\varphi_\nu$  are connected with the rectangular coordinate system,  $(x, y)$ , by the relationships:

$$x = X_\nu + r_\nu \sin \varphi_\nu, \quad y = Y_\nu + r_\nu \cos \varphi_\nu, \quad (3)$$

where  $\nu = 1, 2, \dots, N$ , corresponds to each cylinder.

The following normalisation will be used. In the analysis, all variables and parameters that have the dimension of length are considered normalised (divided) by  $D/\pi$ .

The problem is now reduced to finding fields  $P(x, y)$ ,  $P_{sv}(x, y)$ ,  $F^{(\nu)}(r_\nu, \varphi_\nu)$ , and  $\Phi^{(\nu)}(r_\nu, \varphi_\nu)$ , which satisfy:

(1) Helmholtz equations:

$$(\Delta + k^2)P(x, y) = 0 \quad (4)$$

in the region  $r_\nu \geq R_\nu, 0 \leq x \leq \pi, -\infty < y < \infty$

$$(\Delta + k_{l\nu}^2)\Phi(r_\nu, \varphi_\nu) = 0 \quad (5)$$

$$(\Delta + k_t^2)F(r_\nu, \varphi_\nu) = 0 \quad (6)$$

in the region  $0 \leq r_\nu \leq R_\nu, 0 \leq \varphi_\nu \leq 2\pi$ , where  $\Delta$  is the Laplace operator,  $k = 2D/\lambda$ ,  $k_{l\nu} = kc/c_{l\nu}$ ,  $k_t = kc/c_{t\nu}$ . Velocities of longitudinal and transversal waves  $c_{l\nu}$  and  $c_{t\nu}$  in the elastic material are expressed as  $c_{l\nu} = [(\lambda_\nu + 2\mu_\nu)/\rho_\nu]^{1/2}$ ,  $c_{t\nu} = [\mu_\nu/\rho_\nu]^{1/2}$ .

(2) Boundary conditions on the waveguide walls:

$$\left[ \alpha_0 + \beta_0 \frac{\partial}{\partial x} \right]_{x=\pi} P = 0, \quad (7)$$

$$\left[ \alpha_1 + \beta_1 \frac{\partial}{\partial x} \right]_{x=0} P = 0, \quad (8)$$

where  $\alpha_0$ ,  $\alpha_1$ ,  $\beta_0$ ,  $\beta_1$  are constant numbers which are, in general, complex.

(3) Sommerfeld's radiation condition in both  $y$  directions meaning that there are no sources of the scattered field at infinity.

(4) Coupling conditions joining the total field  $P(x,y)$  with the elastic oscillations of  $N$  cylinders at  $r_v = R_v$ .

They correspond to:

(i) the absence of a tangent component of the stress tensor (the fluid is perfect):

$$\sigma_{r\varphi}^{(v)} \Big|_{r_v=R_v} = \mu_v \left[ \frac{\pi}{D} \right]^2 \left[ 2 \frac{\partial}{\partial r_v} \left( \frac{1}{r_v} \frac{\partial \Phi^{(v)}}{\partial \varphi_v} \right) - k_{iv}^2 F^{(v)} - 2 \frac{\partial^2 F^{(v)}}{\partial r_v^2} \right]_{r_v=R_v} = 0, \quad (9)$$

(ii) the continuity of the normal component of the stress tensor:

$$\sigma_{rr}^{(v)} \Big|_{r_v=R_v} = 2\mu_v \left[ \frac{\pi}{D} \right]^2 \left[ \frac{\partial}{\partial r_v} \left( \frac{1}{r_v} \frac{\partial F^{(v)}}{\partial \varphi_v} \right) - \frac{\lambda_v}{2\mu_v} k_{iv}^2 \Phi^{(v)} + \frac{\partial^2 \Phi^{(v)}}{\partial r_v^2} \right]_{r_v=R_v} = -P \Big|_{r_v=R_v}, \quad (10)$$

(iii) the continuity of the normal component of the displacement vector:

$$u_r^{(v)} \Big|_{r_v=R_v} = \left[ \frac{\pi}{D} \right]^2 \left[ \frac{\partial \Phi^{(v)}}{\partial r_v} + \frac{1}{r_v} \frac{\partial F^{(v)}}{\partial \varphi_v} \right]_{r_v=R_v} = \left[ \frac{1}{\rho (kc)^2} \frac{\partial P}{\partial r_v} \right]_{r_v=R_v}. \quad (11)$$

### 8.3 Solution of the Boundary Value Problem

#### 8.3.1 Representation of the Pressure Field and Elastic Potentials

A solution of the boundary problem is found in the approximation of a given field  $P_e(x,y)$  which may be imagined as a series of complete eigenfunctions,  $P_n(x,y)$  of the boundary value problem (4)-(11). They have the form:

$$P_n(x,y) = \exp(ig_n y) \cdot \sin(\gamma_n x - \theta_n), \quad (12)$$

where

$$g_n = (k^2 - \eta_n^2)^{1/2}. \quad (13)$$

Here  $g_n$  and  $\gamma_n$  are correspondingly longitudinal and transversal wavenumbers. The spectrum of eigenvalues  $\gamma_n$  is determined by the dispersion equation:

$$\tan(\eta_n \pi) = \frac{\xi_1 - \xi_0}{\xi_0 \xi_1 + \eta_n^2} \eta_n, \quad (14)$$

$$\theta_n = \tan^{-1} \left( \frac{\eta_n}{\xi_0} \right), \quad \xi_0 = \frac{\alpha_0}{\beta_0}, \quad \xi_1 = \frac{\alpha_1}{\beta_1}, \quad (15)$$

Eigenfunctions of the corresponding conjugate problem are given by:

$$\bar{P}_n(x,y) = \frac{2}{\gamma_n} P_n^*(x,y), \quad (16a)$$

$$\gamma_n = \pi + \frac{\xi_1 - \xi_0}{(\xi_0 - \eta_n^2)(\xi_1 - \eta_n^2)}, \quad (16b)$$

Using Eq. (12), the field from external sources can be written as a sum of normal modes (eigenfunctions)

$$P_e(x, y) = \sum_{n=1}^{\infty} \bar{A}_n \exp(ig_n y) \sin(\eta_n x - \theta_n), \quad (17)$$

where  $A_n$  are given amplitudes. The incident field may also be represented with respect to the  $(r_v, \varphi_v)$  coordinate system connected with the  $v$ th cylinder:

$$P_e(x, y) = \sum_{m=-\infty}^{\infty} a_{mv} J_m(kr_v) \exp(im\varphi_v), \quad (18)$$

where

$$a_{mv} = i^m \sum_{n=1}^{\infty} A_n \exp(ig_n Y_v) \sin(g_n X_v + m\Psi_v - \theta_n), \quad (19)$$

$$\Psi_n = \cos^{-1}\left(\frac{\eta_n}{k}\right) - \frac{\pi}{2}. \quad (20)$$

The scattered field  $P_s(x, y)$  can be found as a potential of a simple layer:

$$P_s(x, y) = \sum_{v=1}^N P_{sv}(x, y) = \sum_{v=1}^N \int_{L_v} G_v(x, y; x_{v0}, y_{v0}) \mu_v^0(x_{v0}, y_{v0}) dl_{v0}, \quad (21)$$

where  $\mu_v^0(x_{v0}, y_{v0})$  is an unknown function describing the source field distribution on the surface of the  $v$ -th cylinder,  $(x, y)$  are the coordinates of an observation point,  $(x_{v0}, y_{v0})$  are the coordinates of current integration point over the line  $L_v$ , that is a circle of radius  $R_v$ , centred at the point  $x = X_v, y = Y_v$ , and  $dl_{v0}$  is an element of the circle.

The Green's function  $G_v(x, y; x_{v0}, y_{v0})$  is the field radiated by a point source in the waveguide and is the solution of the following equation:

$$(\Delta + k^2)G_v = \delta(x - x_{v0})\delta(y - y_{v0}), \quad v = 1, 2, \dots, N, \quad (22)$$

which fits the radiation condition at  $y \rightarrow \pm\infty$  and the boundary conditions given by Eqs. (7), (8). The Green's function is commonly written in the following form:

$$G_v(x, y; x_{v0}, y_{v0}) = \sum_{n=1}^{\infty} G_{vn}(x, y; x_{v0}, y_{v0}), \quad (23)$$

$$G_n = \frac{i}{\gamma_n g_n} \sin(\eta_n x - \theta_n) \sin(\eta_n x_{v0} - \theta_n) \begin{cases} \exp(ig_n(y - y_{v0})), & y \geq y_{v0} \\ \exp(ig_n(y_{v0} - y)), & y \leq y_{v0} \end{cases}. \quad (24)$$

Since  $dl_{0v} = R_v d\varphi_{0v}$ , denoting  $\mu_v(\varphi_0) = R_v \mu_v^0(\varphi_{v0})$ , it is possible to turn to a single integral over  $\varphi_{0v}$  in Eq. (21):

$$P_{sv} = \int_0^{2\pi} G_v(x, y; R_v, \varphi_{v0}) \mu_v(\varphi_{v0}) d\varphi_{v0}. \quad (25)$$

The use of Green's function in Eq. (21) in the form (23) allows the problem to be reduced to finding a distribution of the sound field sources  $\mu_v^0$  on  $N$  cylinders each, that will fit the continuity conditions (9)-(11).

Distribution of the potentials  $F^{(v)}(r_v, \varphi_v)$  and  $\Phi^{(v)}(r_v, \varphi_v)$  in the elastic cylinders is found as a series of the respective eigenfunctions of a cylinder:

$$F^{(v)}(r_v, \varphi_v) = \sum_{m=-\infty}^{\infty} A_{vm} J_m(k_{lv} r_v) \exp(im\varphi_v), \quad (26a)$$

$$\Phi^{(v)}(r_v, \varphi_v) = \sum_{m=-\infty}^{\infty} B_{vm} J_m(k_{lv} r_v) \exp(im\varphi_v). \quad (26b)$$

### 8.3.2 System of Fredholm Integral Equations.

Substituting the expressions (26) into (9) - (11) gives the following correlations, linking the coefficients  $A_{vm}$  and  $B_{vm}$  with the pressure field on the boundary of the scattering object:

$$A_{vm} = i \frac{\Phi_{1m}(k_{lv} R_v)}{\Phi_{2m}(k_{lv} R_v)} B_{vm}, \quad -\infty < m < \infty, \quad (27)$$

$$\sum_{m=-\infty}^{\infty} z_{1m}^v B_{vm} e^{im\varphi} = \left[ \frac{\partial P_e}{\partial r_v} \right]_{r_v=R_v} + \left[ \frac{\partial P_{sv}}{\partial r_v} \right]_{r_v=R_v}, \quad (28)$$

$$\sum_{m=-\infty}^{\infty} z_{2m}^v B_{vm} e^{im\varphi} = -P_e|_{r_v=R_v} - P_{sv}|_{r_v=R_v} \quad (29)$$

By taking into account the expression (17) for the incident pressure field, it is possible to rewrite the expressions (28) and (29) as follows:

$$\sum_{m=-\infty}^{\infty} [z_{1m}^v B_{vm} - k J'_m(k R_v) a_{mv}] e^{im\varphi} = \left[ \frac{\partial}{\partial r_v} \left( \sum_{l=1}^N P_{sl} \right) \right]_{r_v=R_v}, \quad (30)$$

$$\sum_{m=-\infty}^{\infty} [z_{2m}^v B_{vm} - k J_m(k R_v) a_{mv}] e^{im\varphi} = - \left[ \left( \sum_{l=1}^N P_{sl} \right) \right]_{r_v=R_v}, \quad (31)$$

where  $z_{1m}^v$ ,  $z_{2m}^v$ ,  $\Phi_{1m}(x)$ ,  $\Phi_{2m}(x)$ ,  $\Phi_{3m}(x)$  are determined by expressions:

$$z_{1m}^v = \frac{\rho(kc)^2 (\pi/D)^2}{R_v \Phi_{2m}(k_{lv} R_v)} \times [k_{lv} R_v J'_m(k_{lv} R_v) \Phi_{2m}(k_{lv} R_v) - m J'_m(k_{lv} R_v) \Phi_{1m}(k_{lv} R_v)], \quad (32)$$

$$z_{2m}^v = \frac{\mu_v(\pi/D)^2}{R_v \Phi_{2m}(k_{rv} R_v)} \times \quad (33)$$

$$[\Phi_{3m}(k_{rv} R_v) \Phi_{2m}(k_{rv} R_v) - \Phi_{1m}(k_{rv} R_v) \Phi_{1m}(k_{rv} R_v)],$$

$$\Phi_{1m}(x) = 2m[xJ'_m(x) - J_m(x)], \quad (34)$$

$$\Phi_{2m}(x) = x^2[2J''_m(x) + J_m(x)], \quad (35)$$

$$\Phi_{3m}(x) = 2x^2 \left[ J''_m(x) - \frac{\lambda_v}{2\mu_v} J_m(x) \right]. \quad (36)$$

The right-hand parts of Eqs. (30),(31) contain the sum of  $N$  integrals over lines  $L_v$ . At  $l \neq v$  they are obvious Riemann's integrals. However, at  $l = v$  they are singular, what can be seen from the representation of the scattered field through Green's function (24). At  $l = v$  the integrals make no sense in Riemann's interpretation, but obtain a definite sense by introducing the Cauchy principal value of the integral. If at  $l \neq v$  the fields  $P_{sl}$  and the radial derivatives  $\partial P_{sl}/\partial r_v$  are continuous functions along the line  $L_v$ , at  $l = v$  the derivatives  $\partial P_{sl}/\partial r_v$  have a break of the first kind, which equals  $\mu_v(\varphi_v)$  in magnitude. Thus, the integrals of  $P_{sl}$  in Eq. (25), and the derivatives  $\partial P_{sl}/\partial r_v$  in the right-hand parts of Eq. (30) should be understood in the sense of the principal value. The differentiation operators should be transferred immediately on the function being integrated. In terms of these remarks the correlations (30), (31) can be represented as a system of  $2N$  singular Fredholm integral equations of the second kind relative to the functions  $\mu_v(\varphi_v)$  and the coefficients  $B_{vm}$ :

$$\sum_{m=-\infty}^{\infty} [z_{1m}^v B_{vm} - kJ'_m(kR_v) a_{mv}] \exp(im\varphi_v) = \quad (37a)$$

$$\mu_v(\varphi_v) + \sum_{l=1}^N \int_0^{2\pi} L_{vl}(\varphi_v, \varphi_{l0}) \mu_v(\varphi_{l0}) d\varphi_{l0},$$

$$\sum_{m=-\infty}^{\infty} [z_{2m}^v B_{vm} + kJ_m(kR_v) a_{mv}] \exp(im\varphi_v) = \quad (37b)$$

$$- \sum_{l=1}^N \int_0^{2\pi} K_{vl}(\varphi_v, \varphi_{l0}) \mu_v(\varphi_{l0}) d\varphi_{l0},$$

where

$$K_{vl} = [G_l(x_v, y_v; x_{l0}, y_{l0})]_{r_v=R_v}, \quad (38a)$$

$$L_{vl} = \left[ \frac{\partial}{\partial r_v} G_l(x_v, y_v; x_{l0}, y_{l0}) \right]_{r_v=R_v}, \quad (38b)$$

$$x_v = X_v + R_v \sin \varphi_v, \quad y_v = Y_v + R_v \cos \varphi_v, \quad (39)$$

$$K_{vl} = \sum_{n=1}^{\infty} K_{vl}^n(\varphi_v, \varphi_{l0}), \quad (40a)$$

$$L_{vl} = \sum_{n=1}^{\infty} L_{vl}^n(\varphi_v, \varphi_{l0}), \quad (40b)$$

$$K_{vl}^n = \frac{i}{\gamma_n g_n} \sin(\eta_n x_v - \theta_n) \sin(\eta_n x_{l0} - \theta_n) \exp[ig_n |y_v - y_{l0}|] \quad (41a)$$

$$L_{vl}^n = \frac{\sin(\eta_n x_{l0} - \theta_n)}{\gamma_n} \times \left[ \frac{\eta_n}{ig_n} \sin(\varphi_v) \cos(\eta_n x_v - \theta_n) \pm \cos(\varphi_v) \sin(\eta_n x_v - \theta_n) \right] \times \exp[ig_n |y_v - y_{l0}|], \quad (41b)$$

$$x_{l0} = X_l + R_l \sin \varphi_{l0}, \quad y_{l0} = Y_l + R_l \cos \varphi_{l0}. \quad (42)$$

Here the top sign corresponds to the region  $y_v \geq y_{l0}$ , and the lower sign corresponds to the region  $y_v \leq y_{l0}$ .

### 8.3.3 Improving Convergence of the Green's function.

It is known that integral formulations using the Green's function have convergence difficulties in waveguides. Indeed, if  $v = l$  and  $\varphi_0 \approx \varphi_v$  the exponential term in formulas (41) decreases slowly when waveguide mode number  $n$  grows, and the Green's function and its radial derivative described by the expressions (38)-(42) converge very slowly. This fact leads to the necessity of taking into account extremely high numbers of terms in the series (40), that dramatically increases time and degrades the accuracy of computer calculations. That is why the use of such a model in waveguides requires truncation of the series at some  $n$ , commonly evanescent modes are ignored and only propagating modes are retained. Solutions, which are obtained using such truncated series, are believed to be valid only for large distances from the scattering objects (Wu, 1994). However, as will be shown in this work, such solutions are not correct even for large distances, because the boundary conditions on the surface of the object must include the evanescent modes along with these, which propagate. To overcome this difficulty, the following improvement of the convergence of the Green's function is proposed.

It will be convenient to add and subtract the following functions  $\bar{K}_{vl}(\varphi_v, \varphi_{0l})$  and  $\bar{L}_{vl}(\varphi_v, \varphi_{0l})$  to and from the functions  $K_{vl}$  and  $L_{vl}$  as follows:

$$K_{vl} = \bar{K}_{vl} + K_{vl} - \bar{K}_{vl}, \quad L_{vl} = \bar{L}_{vl} + L_{vl} - \bar{L}_{vl}, \quad (43)$$

where  $\bar{K}_{vl}$  and  $\bar{L}_{vl}$  are defined by the following expressions:

$$\bar{K}_{\nu l} = \sum_{n=1}^{\infty} \bar{K}_{\nu l}^n, \quad \bar{L}_{\nu l} = \sum_{n=1}^{\infty} \bar{L}_{\nu l}^n, \quad (44)$$

$$\bar{K}_{\nu l}^n = K_{\nu l}^n + O(n^{-2}), \quad \bar{L}_{\nu l}^n = L_{\nu l}^n + O(n^{-2}). \quad (45)$$

Now the Green's function  $K_{\nu l}$  and its derivative  $L_{\nu l}$  on the boundary of the  $\nu$ -th cylinder can be written as follows:

$$K_{\nu l} = \bar{K}_{\nu l} + \sum_{n=1}^{\infty} (K_{\nu l}^n - \bar{K}_{\nu l}^n), \quad L_{\nu l} = \bar{L}_{\nu l} + \sum_{n=1}^{\infty} (L_{\nu l}^n - \bar{L}_{\nu l}^n). \quad (46)$$

The formulas (46) allow one to calculate the value of the Green's function and its derivative easily. The first term in the formulas does not depend on the mode order  $n$ , and so, it describes the influence of all higher-order evanescent modes. It can also easily be proved that the series are quickly convergent. According to the formulas (45), one of the terms in the series tends to the other one as  $n$  increases. The functions  $K_{\nu l}$  and  $L_{\nu l}$  are defined differently for every set of boundary conditions, and their expressions for the two cases considered are shown below.

The first set of boundary conditions, considered in the current work, corresponds to the asymmetric waveguide, with a pressure release top surface and an absolutely rigid bottom ( $\alpha_0 = \beta_1 = 0$ ). The functions, describing the waveguide Green's function and its derivative along the direction  $\varphi$ , take the following form:

$$\eta_n = n + \frac{1}{2}, \quad \gamma_n = \pi, \quad \theta_n = \pi/2, \quad g_n = \sqrt{k^2 - (n + \frac{1}{2})^2}, \quad n = 0, 1, 2, \dots \quad (47)$$

$$K_n = \frac{i}{\pi g_n} \cos(n + \frac{1}{2})x_0 \cos(n + \frac{1}{2})x \exp(ig_n |y - y_0|), \quad (48a)$$

$$L_n = \frac{1}{\pi} \cos(n + \frac{1}{2})x_0 \left[ \frac{n + \frac{1}{2}}{ig_n} \sin \varphi \sin(n + \frac{1}{2})x \mp \cos \varphi \cos(n + \frac{1}{2})x \right] \times \exp(ig_n |y - y_0|), \quad (48b)$$

$$\bar{K}_n = \frac{1}{\pi(n + \frac{1}{2})} \cos(n + \frac{1}{2})x_0 \cos(n + \frac{1}{2})x \exp[-(n + \frac{1}{2})|y - y_0|], \quad (49a)$$

$$\bar{L}_n = \frac{1}{\pi} \left( 1 + \frac{k^2}{2n + 1} |y - y_0| \right) \cos(n + \frac{1}{2})x_0 \times [-\sin \varphi \sin(n + \frac{1}{2})x \mp \cos \varphi \cos(n + \frac{1}{2})x] \exp[-(n + \frac{1}{2})|y - y_0|], \quad (49b)$$

$$\bar{K} = \frac{1}{4\pi} \ln \left[ \frac{\cosh \frac{1}{2}|y - y_0| + \cos \frac{1}{2}(x - x_0)}{\cosh \frac{1}{2}|y - y_0| - \cos \frac{1}{2}(x - x_0)} \times \frac{\cosh \frac{1}{2}|y - y_0| + \cos \frac{1}{2}(x + x_0)}{\cosh \frac{1}{2}|y - y_0| - \cos \frac{1}{2}(x + x_0)} \right], \quad (50a)$$



$$\begin{aligned}
 \bar{L} = & \frac{1}{2\pi} \left\{ -\sin \varphi \left[ \frac{\sin \frac{1}{2}(x-x_0) \cosh \frac{1}{2}|y-y_0|}{\cosh|y-y_0| - \cos(x-x_0)} + \frac{\sin \frac{1}{2}(x+x_0) \cosh \frac{1}{2}|y-y_0|}{\cosh|y-y_0| - \cos(x+x_0)} \right] \right. \\
 & \mp \cos \varphi \sinh \frac{1}{2}|y-y_0| \left[ \frac{\cos \frac{1}{2}(x-x_0)}{\cosh|y-y_0| - \cos(x-x_0)} + \frac{\cos \frac{1}{2}(x+x_0)}{\cosh|y-y_0| - \cos(x+x_0)} \right] \quad (50b) \\
 & + \frac{1}{2}k^2|y-y_0| \left[ -\sin \varphi \left( \arctan \frac{\sin \frac{1}{2}(x-x_0)}{\sinh \frac{1}{2}|y-y_0|} + \arctan \frac{\sin \frac{1}{2}(x+x_0)}{\sinh \frac{1}{2}|y-y_0|} \right) \right. \\
 & \left. \mp \frac{1}{2} \cos \varphi \ln \left( \frac{\cosh \frac{1}{2}|y-y_0| + \cos \frac{1}{2}(x-x_0)}{\cosh \frac{1}{2}|y-y_0| - \cos \frac{1}{2}(x-x_0)} \times \frac{\cosh \frac{1}{2}|y-y_0| + \cos \frac{1}{2}(x+x_0)}{\cosh \frac{1}{2}|y-y_0| - \cos \frac{1}{2}(x+x_0)} \right) \right] \left. \right\}.
 \end{aligned}$$

The second set of boundary conditions corresponds to a symmetric waveguide, with two pressure release boundaries ( $\beta_0 = \beta_1 = 0$ ). The functions in this case take the following form:

$$\eta_n = n, \gamma_n = \pi, \theta_n = 0, g_n = \sqrt{k^2 - n^2}, n = 1, 2, \dots \quad (51)$$

$$K_n = \frac{i}{\pi g_n} \sin nx_0 \sin nx \exp(ig_n|y-y_0|), \quad (52a)$$

$$L_n = \frac{1}{\pi} \sin nx_0 \left[ -\frac{n}{ig_n} \sin \varphi \cos nx \mp \cos \varphi \sin nx \right] \times \exp(ig_n|y-y_0|), \quad (52b)$$

$$\bar{K}_n = \frac{1}{\pi n} \sin nx_0 \sin nx \exp[-n|y-y_0|], \quad (53a)$$

$$\bar{L}_n = \frac{1}{\pi} \left( 1 + \frac{k^2}{2n} |y-y_0| \right) \sin nx_0 [\sin \varphi \cos nx \mp \cos \varphi \sin nx] \exp[-n|y-y_0|], \quad (53b)$$

$$\bar{K} = \frac{1}{4\pi} \ln \left[ \frac{\cosh|y-y_0| - \cos(x+x_0)}{\cosh|y-y_0| - \cos(x-x_0)} \right], \quad (54a)$$

$$\begin{aligned}
 \bar{L} = & \frac{1}{4\pi} \left\{ \sin \varphi \left[ \frac{\sin(x_0-x)}{\cosh|y-y_0| - \cos(x_0-x)} + \frac{\sin(x+x_0)}{\cosh|y-y_0| - \cos(x+x_0)} \right] \right. \\
 & \mp \cos \varphi \left[ \frac{\cos(x_0-x) - e^{-|y-y_0|}}{\cosh|y-y_0| - \cos(x_0-x)} - \frac{\cos(x+x_0) - e^{-|y-y_0|}}{\cosh|y-y_0| - \cos(x+x_0)} \right] \quad (54b) \\
 & + k^2|y-y_0| \left[ \sin \varphi \left( \arctan \frac{\sin(x_0-x)e^{-|y-y_0|}}{1 - e^{-|y-y_0|} \cos(x_0-x)} \right) \right. \\
 & \left. + \arctan \frac{\sin(x_0+x)e^{-|y-y_0|}}{1 - e^{-|y-y_0|} \cos(x_0+x)} \right] \mp \frac{\cos \varphi}{2} \ln \left( \frac{\cosh|y-y_0| - \cos(x+x_0)}{\cosh|y-y_0| - \cos(x-x_0)} \right) \left. \right\}.
 \end{aligned}$$

In both cases the top sign corresponds to  $y > y_0$ , while the bottom sign corresponds to  $y < y_0$ . The observation and the source points in the waveguide are  $(x, y)$  and  $(x_0, y_0)$ .

The above formulas, used together with formulas (46), provide quickly converging expressions for the Green's function and its derivative, which can be used in many integral formulations of scattering problems in waveguides with specified boundary conditions.

All the calculations, involved in the separation of the asymptotic terms for the symmetric waveguide, are shown in the Appendix A. The calculations for the asymmetric waveguide are analogous.

### 8.3.4 System of Linear Equations.

Now, after the new form of the Green's function has been found, it is possible to find a solution to the boundary value problem, which takes into account ALL the waveguide modes.

The Galerkin-Ritz method with basis function  $\exp(im\varphi_\nu)$  is used to solve the system of equations. Because the functions  $\mu_\nu(\varphi_\nu)$  are determined on the interval  $0 \leq \varphi_\nu \leq 2\pi$  and the integrals  $\int_0^{2\pi} |\mu_\nu(\varphi_\nu)| d\varphi_\nu$  exist due to finiteness of the field  $P_{s\nu}$ , they can be represented as Fourier series:

$$\mu_\nu(\varphi_\nu) = \sum_{p=-\infty}^{\infty} b_{p\nu} \exp(ip\varphi_\nu), \quad b_{p\nu} = \frac{1}{2\pi} \int_0^{2\pi} \mu_\nu(\varphi_\nu) \exp(ip\varphi_\nu) d\varphi_\nu. \quad (55)$$

After substitution of the expressions into Eqs. (37), they must be multiplied by the functions  $\exp(im\varphi_\nu)/2\pi$  and integrated over  $\varphi_\nu$  from 0 to  $2\pi$ . As a result, an inhomogeneous infinite system of linear algebraic equations relative to the coefficients  $b_{p\nu}$  and  $B_{p\nu}$  is obtained. The system can be expressed as:

$$\begin{cases} z_{1m}^\nu B_{vm} - b_{vm} - \sum_{l=1}^N \left[ \sum_{p=-\infty}^{\infty} b_{pl} \Lambda_{pm}^{l\nu} \right] = kJ'_m(kR_\nu) a_{m\nu} \\ z_{2m}^\nu B_{vm} + \sum_{l=1}^N \left[ \sum_{p=-\infty}^{\infty} b_{pl} K_{pm}^{l\nu} \right] = -J_m(kR_\nu) a_{m\nu} \end{cases}, \quad (56)$$

where  $\nu = 1, 2, \dots, N$ ,  $-\infty < m < \infty$  and the matrix elements  $K_{pm}^{l\nu}$  and  $\Lambda_{pm}^{l\nu}$  are determined by:

$$K_{pm}^{l\nu} = \frac{1}{2\pi} \int_0^{2\pi} \left\{ \int_0^{2\pi} K_{\nu l}(\varphi_\nu, \varphi_{l0}) \exp[i(p\varphi_{l0} - m\varphi_\nu)] d\varphi_{l0} \right\} d\varphi_\nu, \quad (57)$$

$$\Lambda_{pm}^{l\nu} = \frac{1}{2\pi} \int_0^{2\pi} \left\{ \int_0^{2\pi} L_{\nu l}(\varphi_\nu, \varphi_{l0}) \exp[i(p\varphi_{l0} - m\varphi_\nu)] d\varphi_{l0} \right\} d\varphi_\nu. \quad (58)$$

The comparison of Eqs. (56) with Eqs. (28) and (29) gives the following expressions for the scattered field and its radial derivative on the surface of  $\nu$ -th cylinder:

$$P_{s\nu}(R_\nu, \varphi_\nu) = \sum_{m=-\infty}^{\infty} \sum_{l=1}^N \sum_{p=-\infty}^{\infty} b_{pl} K_{pm}^{l\nu} e^{im\varphi_\nu}, \quad (59)$$

$$\frac{\partial P_{sv}(R_\nu, \varphi_\nu)}{\partial r_\nu} = \sum_{m=-\infty}^{\infty} \left[ b_{vm} + \sum_{l=1}^N \left( \sum_{p=-\infty}^{\infty} b_{pl} \Lambda_{pm}^{lv} \right) \right] e^{im\varphi_\nu}. \quad (60)$$

In the above formulas the index  $m$  corresponds to the Fourier coefficients of the scattered field on the surface of  $\nu$ -th cylinder, the index  $l$  corresponds to  $l$ -th cylinder. The index  $p$  corresponds to the contribution of the  $p$ -th Fourier component of the acoustic source distribution to the Fourier components of the scattered field on the surface of  $\nu$ -th cylinder. The sum over  $p$  shows that all components of the scattered field on the cylinder surface are coupled with each other through the boundary conditions.

The functions  $K_{vl}(\varphi_\nu, \varphi_{l0})$ ,  $L_{vl}(\varphi_\nu, \varphi_{l0})$  are the improved Green's function and its derivative respectively, defined by Eqs. (46). The angle  $\varphi_\nu$  is the angular position of an observation point on the surface of the  $\nu$ -th cylinder, and the angle  $\varphi_{l0}$  is the angular position of a source point on the surface of the  $l$ -th cylinder.

Elimination of the coefficients  $B_{vm}$  from the system (56) allows formulation of the following system of linear equations:

$$b_{vm} + \sum_{l=1}^N \left[ \sum_{p=-\infty}^{\infty} b_{pl} M_{pm}^{lv} \right] = P_{pm}^v a_{m\nu}. \quad (61)$$

The coefficients  $B_{vm}$ , describing the  $z$ -component of the vector elastic potential in the  $\nu$ -th cylinder, are determined by the expression:

$$B_{vm} = -\frac{1}{z_{2m}^v} \left[ J_m(kR_\nu) a_{m\nu} + \sum_{l=1}^N \left[ \sum_{p=-\infty}^{\infty} b_{pl} K_{pm}^{lv} \right] \right]. \quad (62)$$

The scattering matrix elements  $M_{pm}^{lv}$  are determined by the following double integral:

$$M_{pm}^{lv} = \Lambda_{pm}^{lv} + z_{vm} K_{pm}^{lv} = \frac{1}{2\pi} \int_0^{2\pi} \left\{ \int_0^{2\pi} [L_{vl}(\varphi_\nu, \varphi_{l0}) + z_{vm} K_{vl}(\varphi_\nu, \varphi_{l0})] \exp[i(p\varphi_{l0} - m\varphi_\nu)] d\varphi_{l0} \right\} d\varphi_\nu, \quad (63)$$

where impedances  $z_{vm}$  are defined by:

$$z_{vm} = \frac{z_{1m}^v}{z_{2m}^v}. \quad (64)$$

The coefficients  $P_{pm}^v$ , determining the right-hand part of Eq. (61), can be found as:

$$P_{pm}^v = -(kJ'_m(kR_\nu) + z_{vp} J_m(kR_\nu)) \delta_{pm}, \quad (65)$$

where  $\delta_{pm}$  is the Kronecker's symbol.

The formula (63) requires integration of the functions  $L$  and  $K$  twice over the surface of the cylinder. The appearance of these functions for the two sets of boundary conditions considered in this work, are represented by the formulas (46) – (54). In the case of one cylinder, the coordinates of the point of observation,  $(x, y)$ , and the source point,  $(x_0, y_0)$ , are connected with  $\varphi$  and  $\varphi_0$  in the following way:

$$x = H + R_0 \sin \varphi, \quad y = Y_0 + R_0 \cos \varphi, \quad (66)$$

$$x_0 = H + R_0 \sin \varphi_0, \quad y_0 = Y_0 + R_0 \cos \varphi_0. \quad (67)$$

Here,  $H$ ,  $Y_0$  and  $R_0$  are, respectively, the distance between the cylinder centre and the bottom, the horizontal coordinate of the cylinder centre, and the external radius. In the case of multiple cylinders, the points  $(x,y)$  and  $(x_0, y_0)$  may also belong to the surfaces of different cylinders.

To calculate the matrix elements  $M_{pm}^{lv}$ , the integral (63) must be evaluated numerically. However, direct numerical calculation of the integral is impossible, due to the singularities in the functions  $\bar{K}_{vl}(\varphi_v, \varphi_{l0})$  and  $\bar{L}_{vl}(\varphi_v, \varphi_{l0})$  at  $v=l$  and  $\varphi_v = \varphi_{l0}$  (see formulas (50) and (54)). To proceed, a small  $\varepsilon$ -strip near the line  $\varphi_v = \varphi_{l0}$ , which contains the singularity, is separated and the integral over this strip is evaluated analytically. All the necessary calculations for the case of the symmetric waveguide are shown in the Appendix B.

When the matrix elements are calculated, solution of the system of equations (61) permits one to calculate the distribution of the field  $P(x,y)$  using the following formula:

$$P_s(x, y) = \sum_{v=1}^N \sum_{p=-\infty}^{\infty} \int_0^{2\pi} b_{pv} G_v(x, y; x_{v0}, y_{v0}) \exp(ip\varphi_{v0}) d\varphi_{v0}. \quad (68)$$

Asymptotic ( $k \rightarrow 0$ ) parts must be also separated in the expressions of Green's function  $G_v$ .

The distributions of the potentials  $F^{(v)}(r_v, \varphi_v)$  and  $\Phi^{(v)}(r_v, \varphi_v)$  can be easily calculated by Eqs. (26), (27) and (62).

#### 8.4 Numerical Solution.

Due to the complexity of the expression under the double integral in (63), the matrix elements have to be calculated numerically. The system of linear equations (61) also requires numerical solution. In this work, all the necessary numerical calculations are carried out using Microsoft FORTRAN-77 on personal IBM computers.

The matrix elements are calculated with the use of the 10-point Gauss quadrature formula (Press *et al*, 1988, p.122), which gives exact values to integrals of polynomials up to degree 19. This formula has been chosen as having better accuracy with the same number of integration points after experimental investigation of several algorithms of numerical integration. The actual number of points on

the interval of integration depends upon the frequency and other parameters and varies from 10 to 30.

The appearance of the scattering matrix reveals an important feature of the Multi-Modal Integral Method. Regardless of the infinity of the matrix in both directions, at all sets of parameters considered in this work, the value of the matrix elements tends to zero when the indices increase. Consequently, the matrix can be easily truncated without losing information about the scattering process. The appearance of the matrix and methods of accuracy control used in this work are discussed in detail in Chapter 14.

The system of linear equations (61) is solved by elimination using the largest pivotal divisor. This method produced correct results even when the coefficients of the system differed from each other by several orders of magnitude.

The values of the non-dimensional wavenumber  $k$ , used in the calculations, are chosen to avoid exact coincidence with the critical frequencies of the waveguide modes. At these frequencies, the Green's function has singularities due to the absence of viscous damping in this model.

In general, the numerical implementation of the Multi-Modal Integral Method does not require significant computer resources.

### **8.5 Conclusions.**

A boundary value problem has been formulated for the scattering of sound waves in a two-dimensional waveguide by a set of elastic cylinders. The scattered pressure field is modelled as radiated by a simple source distribution using the waveguide Green's function, the incident wave is considered as known. By substituting the expressions for the pressure field into the boundary conditions, the problem is reduced to a system of Fredholm integral equations, which, in turn, is transformed to an infinite system of linear equations by the Galerkin-Ritz method. Elements of the system matrix are expressed through integrals over the waveguide Green's function.

The Green's function is transformed into the sum of a quickly converging series and a function, which does not depend upon the mode number  $n$ . This new form of the Green's function takes into account all waveguide modes up to infinite order, so permitting accurate and numerically efficient solution of the boundary value problem.

The methodology described in this chapter combines advantages of the eigenfunctions and the integral equations methods. The transformed Green's function for the waveguide makes it possible to solve the complex scattering problem efficiently and with high accuracy. The numerical implementation of the methodology requires few computer resources and can be carried out on an ordinary personal computer.

## 9 Homogeneous Cylinders in Asymmetric Waveguide.

### 9.1 Introduction.

This Chapter describes modelling results obtained for scattering by a homogeneous cylinder in a waveguide with asymmetric boundary conditions (Belov *et al*, 1998). The following two cases are considered:

1. One cylinder in the middle of the waveguide.
2. Two cylinders in the middle of the waveguide at a distance of  $D/2\pi$  between their centres.

### 9.2 Parameters of the System.

Parameters of the system used in the calculations are:

- Boundary conditions:
  - soft upper boundary ( $\alpha_0 \neq 0, \beta_0 = 0$ )
  - rigid bottom ( $\alpha_1 = 0, \beta_1 \neq 0$ )
- Incident wave:
  - amplitude of the lowest mode: 1.
  - amplitudes of higher modes: 0.
- Fluid:
  - Density: 1000 kg/m
  - Sound speed: 1493 m/s
- Cylinders:
  - Diameter: Depth / 10
  - Density: 7700kg/m
  - Lamé coefficients:  
 $\lambda_{1,2} = 2.22 * 10^8$  Pa,  $\mu_{1,2} = 16 * 10^8$  Pa.
- Non-dimensional frequency  $1 < k < 12.5$  ( $k = 2D/\lambda$ , where  $D$  is the waveguide depth).

### 9.3 Amplitude-Frequency Characteristics (AFC)

Amplitude-frequency and phase-frequency characteristics are obtained for coefficients of waveguide modes in the reflected and transmitted field (Belov *et al*, 1998). AFC for the lowest six modes for one cylinder located in the middle of the waveguide are shown on the Fig. 3. Figure 4 represents AFC for the case of two cylinders located one behind the other.

The AFC curves show the following:

1. Near the critical frequency of each waveguide mode  $k_s = n + 0.5$ , a sharp increase of its amplitude and great advance of its phase are observed. There are no appreciable changes of the amplitudes and phases of other modes in this case. This is explained by a sharp increase of the density of the mode energy, because of the multiple reflection at waveguide walls. These phenomena were first observed in optics when light waves are scattered by diffraction gratings, and they are called the Wood's anomalies.
2. Sharp changes of the amplitudes of the waveguide modes occur near natural or resonance frequencies  $k_s \neq n + 0.5$  of the waveguide system. In the first case, such changes were observed in one mode characteristics, but here they take place in the AFC and PFC of all waveguide modes. In this last case resonance oscillations of elastic cylinders with a high quality factor are excited near the resonance frequencies. For their existence, "participation" of all waveguide modes of the system is necessary. The values of the eigenfrequencies  $k_s$  and of the quality factor value, which determines the nature of the changes of the mode amplitudes and phases, mainly depends on geometric and material parameters of the waveguide and the elastic bodies.
3. In both versions of the system, in transmitted and reflected waves the amplitudes of both propagating and non-propagating modes are considerably different from zero, especially in the region of resonance scattering. It means, that nonpropagating modes play an important role, where the field is formed in the area near the scattering objects. It is necessary to consider them for determination of the propagating mode amplitudes in the far field zone.
4. In general, the eigenfrequency spectrum also depends on the number and mutual location of the elastic cylinders. It is easy to determine the values of the natural and resonance frequencies  $k_s$  for each version by AFC and PFC curves. It is necessary to note that in the two cases considered here the spectra ( $k_{sn}$ ) contain eigenfrequencies which are practically the same for both (for example,  $k_s \approx 5.3$ ).

#### **9.4 Phase-Frequency Characteristics (PFC).**

The PFC curves are shown in Figs. 5 and 6. Their main feature is a great advance of the phase of the modes near the resonance frequencies where the mode amplitudes have the sharp increase.

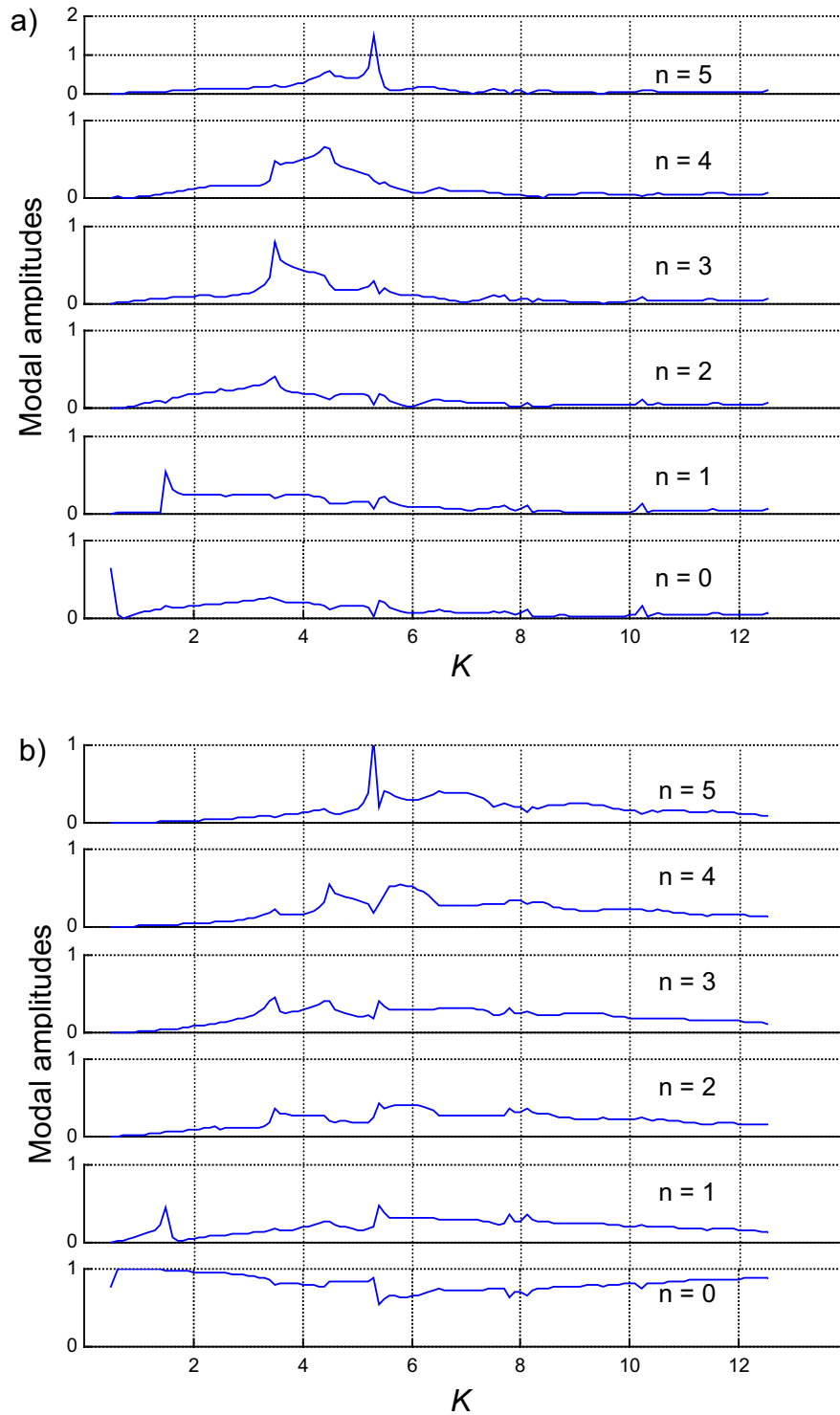


Figure 3. Amplitude-frequency characteristics for one cylinder in the middle of the waveguide. a)reflected wave; b)transmitted wave.



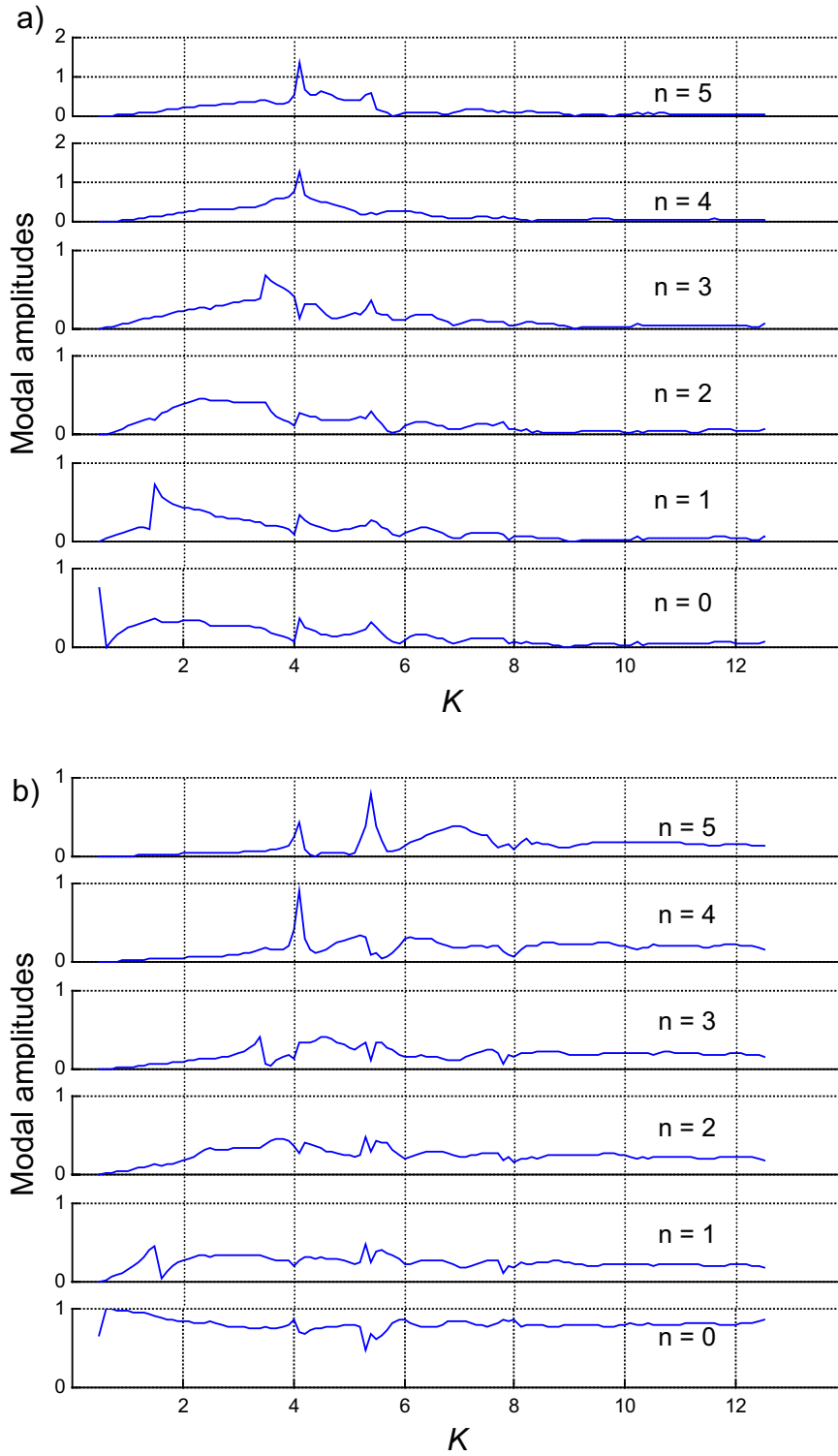


Figure 4 . Amplitude-frequency characteristics for two cylinders in the middle of the waveguide. a)reflected wave; b)transmitted wave.

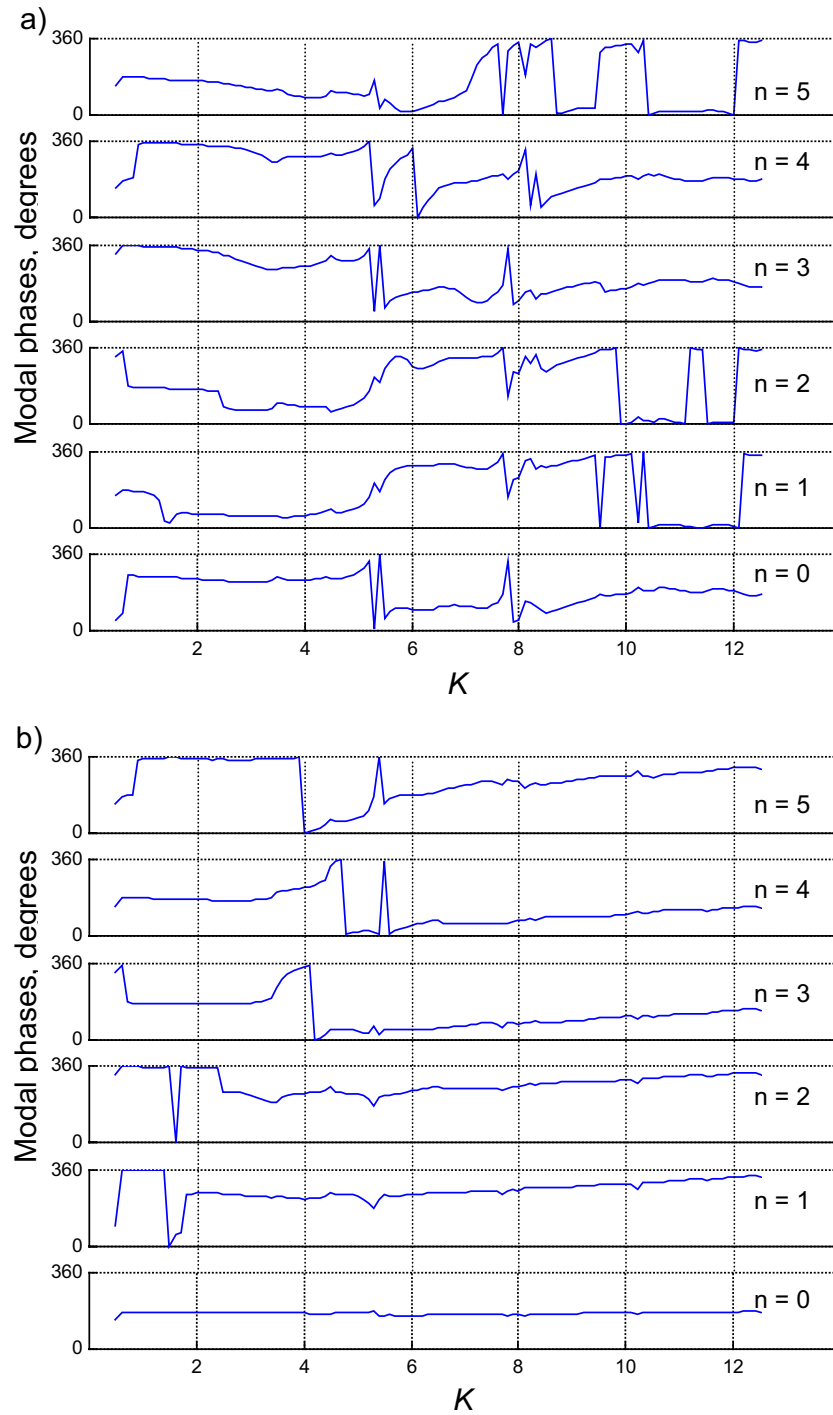


Figure 5. Phase-frequency characteristics for one cylinder in the middle of the waveguide. a)reflected wave; b)transmitted wave.

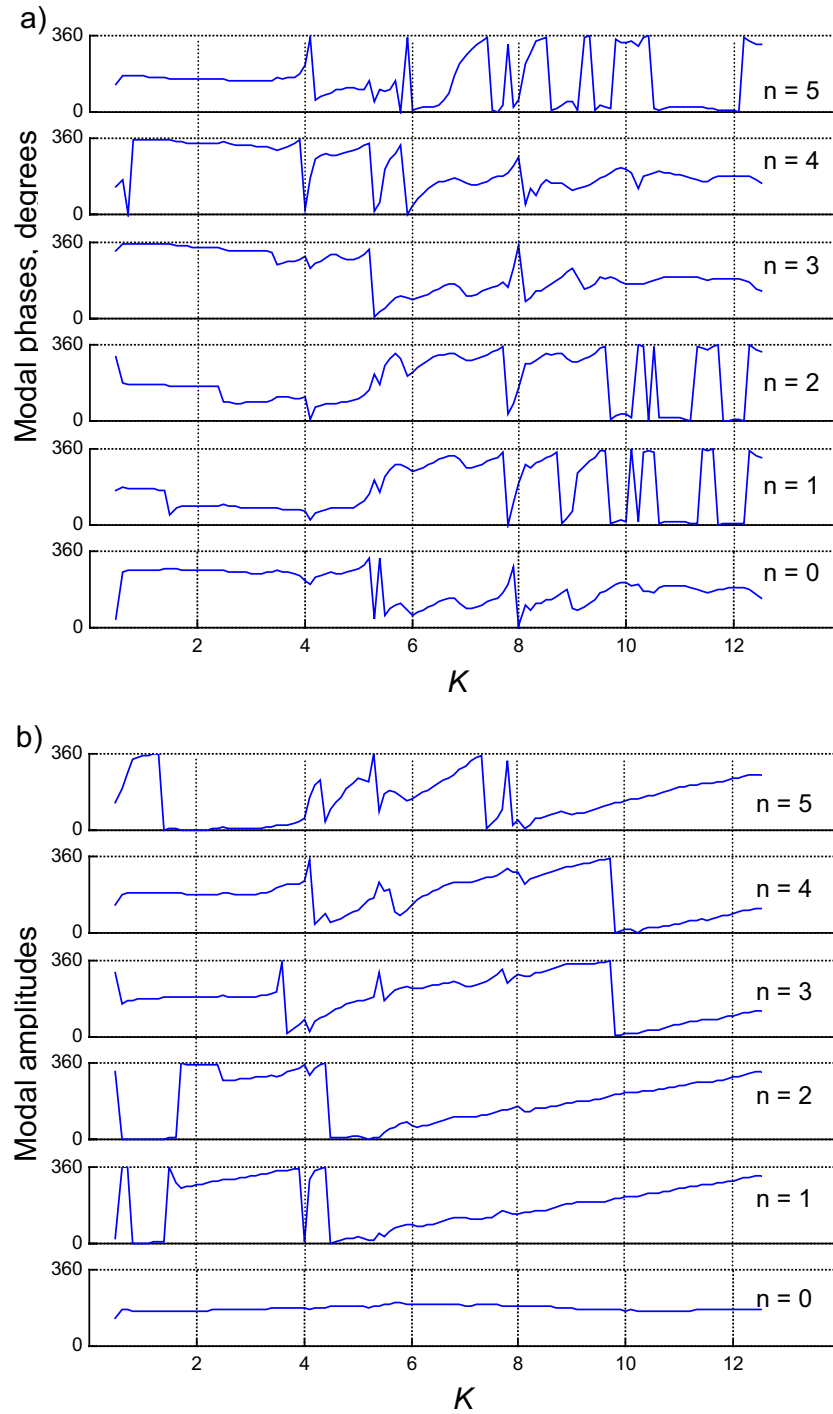


Figure 6. Phase-frequency characteristics for two cylinders in the middle of the waveguide. a) reflected wave; b) transmitted wave.

### 9.5 The Spatial Distribution of the Absolute Value of Pressure Amplitude.

Figs. 7 and 8 show the distribution of the absolute value of the amplitude of the full field,  $P(x,y)$ , calculated using Eqs. (17) and (68) at two close frequencies (wavenumbers). The incident wave comes from the left, the scattering cylinders are depicted by blue circles in the correct scale, and the colour bar shows values compared to the amplitude of the incident wave at the bottom. It should be noted that the values shown in the pictures are always positive, because they represent the absolute value, or the module, of the complex pressure amplitude.

Fig. 7 shows the picture for  $k = 5.301$ , which corresponds to the jump of all waveguide modes in Figs. 3 and 4. It is clearly seen that in the area to the left from the cylinders the incident and the scattered waves, propagating in opposite directions, cause the appearance of a standing wave. Meantime, near the scattering objects the acoustic pressure reaches values 3 to 4 times higher than the amplitude of the incident field. Due to the structure of the incident wave the ratio between the amplitudes of the total and the incident waves near the cylinders will be even higher. In Fig 7b an area of high amplitude can easily be distinguished between the cylinders. This fact confirms again that the amplitude of the higher-order waveguide modes can reach very high values near scattering objects.

The role of higher-order modes can be seen even better when Figs. 7 and 8 are compared. Fig. 8 shows pictures for the same configurations of the waveguide system as for Fig. 4, but for a different, though close frequency  $k = 5.001$ , which lies out of the resonance area. The figure shows, that there are no maxima in the total field near the scattering objects in this case. Maximum of the pressure amplitude is reached near the bottom of the waveguide, according to the boundary conditions. The significant difference of the resonant and non-resonant pictures for one cylinder in Fig. 7a and 8a shows that excitation of higher-order modes near scattering objects can significantly affect the scattered field in the far zone.

Comparison of all four pictures shows an interesting fact: three of them, namely, 7b, 8a and 8b are quite similar in the far field zone. Taking into account the *minima* of the amplitude of the modes propagating in a backward direction in the picture for one cylinder (Fig. 3a), it is possible to suggest the following mechanism. Resonant oscillations of the cylinder cause a *decrease* in the amount of reflected energy in comparison with non-resonant scattering. In other words, the resonant cylinder more effectively transmits acoustic energy, than a non-resonant one. However, in the case of two cylinders, the acoustic energy, transmitted by the first cylinder, is reflected back by the second cylinder. The second cylinder oscillates differently from the first cylinder due to the difference in structure of the incident field in its vicinity because of the field scattered by the

first cylinder. That is why the second cylinder actually *reflects* acoustic energy rather than transmits it. Such behaviour of the second cylinder leads to an overall increase in the amount of acoustic energy reflected back, and the pictures of resonant scattering by two cylinders are similar to the pictures of non-resonant scattering. This phenomenon can be understood by taking into account the phase shift between the vibrations of the cylinders. At the frequency, corresponding to  $k \approx 5$  the acoustic wavelength is approximately twice as big as the distance between the cylinder centres. This suggests that the cylinders oscillate in opposite phase, in which case resonance terms in the scattered field are mutually cancelled. Consequently, the two cylinders scatter the acoustic wave similarly to the single non-resonant cylinder.

This shows that the observed resonances are not determined by the properties of just one cylindrical scattering object, but by the properties of the whole scattering system, consisting of the scattering objects and the waveguide itself.

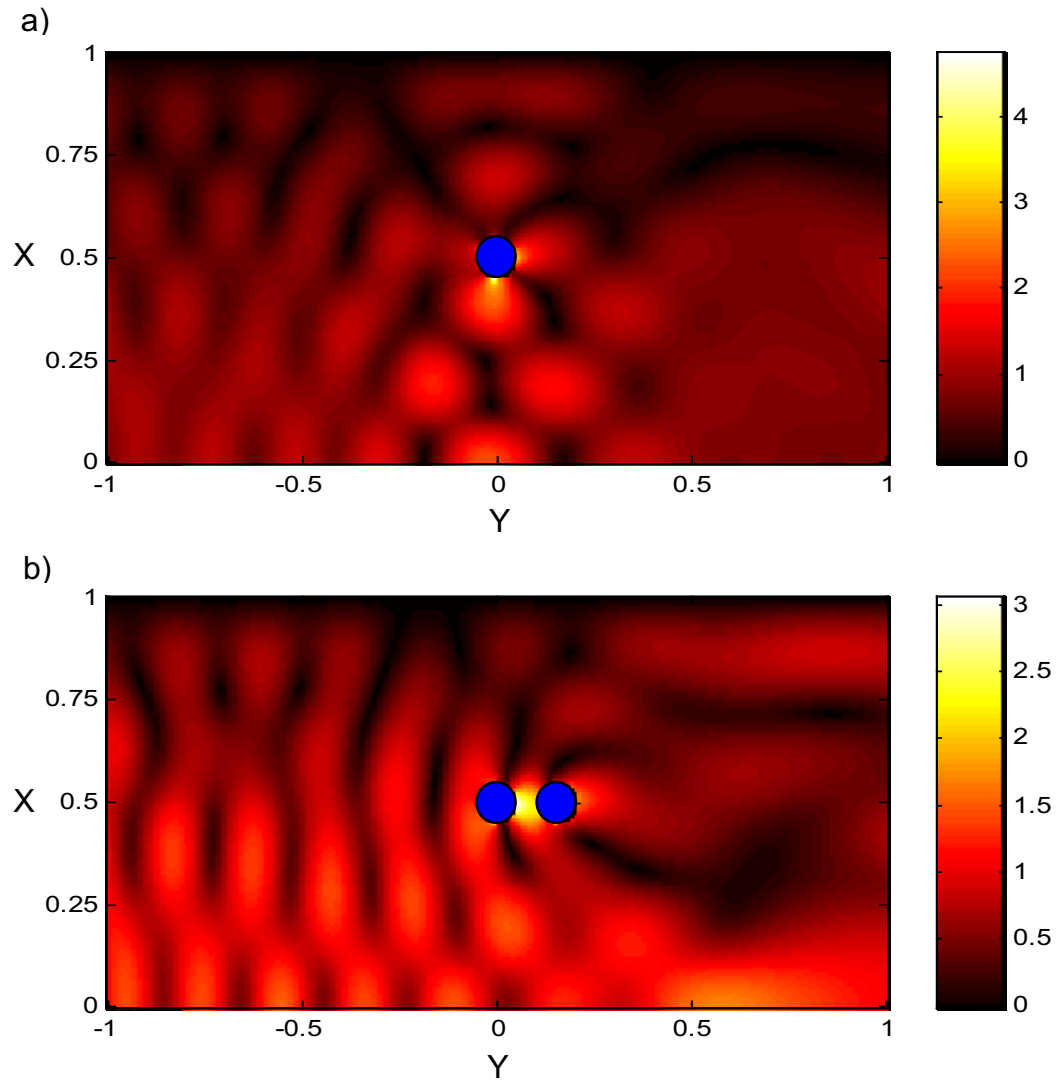


Figure 7. Resonance distribution of the pressure amplitude in the waveguide ( $k = 5.301$ ), a) one cylinder; b) two cylinders. Field incidence is from the left.

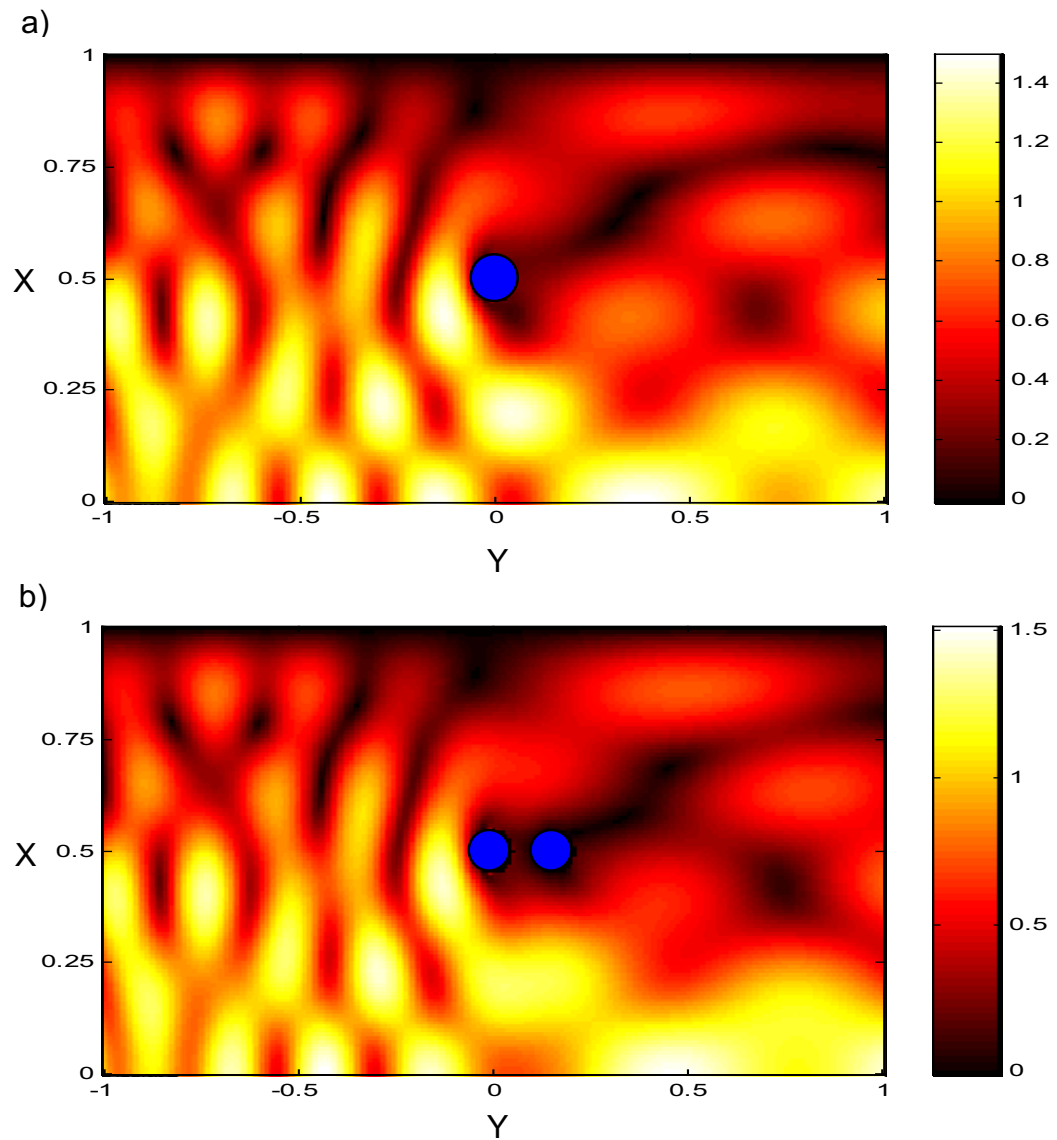


Figure 8. Non-resonance distribution of the pressure amplitude in the waveguide ( $k = 5.001$ ), a) one cylinder; b) two cylinders. Field incidence is from the left.

### 9.6 Source Density on the Cylinder Surface.

Fig. 6 shows the dependence of the density of sources of acoustic waves, described by the function  $\mu_\nu(\varphi_{0\nu})$ , on the angle  $\varphi_{0\nu}$  and non-dimensional wavenumber (frequency)  $k$ . The top picture corresponds to the case of one cylinder. Its analysis reveals that the function  $\mu_\nu(\varphi_{0\nu})$  in this case experiences resonances at the following frequencies:  $k_1 = 5.3$ ,  $k_2 = 8.1$ ,  $k_3 = 10.2$ , and  $k_4 = 10.5$ . The first three resonances have correspondingly four, six and eight distinct maxima in their spatial configuration, so that they can be physically associated with structural modes of the cylinder or surface elastic waves of some type. The corresponding mode numbers are, apparently, two, three, and four. The fourth resonance has the same number of maxima as the third one, but it is spatially shifted by half a wavelength. This resonance appears to be not a separate resonance, but, together with the third one, it represents a single resonance split in two due to the influence of the waveguide boundaries. Indeed, in a waveguide none of the structural modes of the cylinder can be considered as independent oscillators. Instead, they are coupled to each other by multiple reflections of the sound radiated by them from the waveguide boundaries. In a free unbounded fluid, such a split may be observed only if two or more scattering objects are located close to each other. This was demonstrated by Lethullier *et al* (1998) by the example of two cylindrical shells.

In the case of two cylinders (see Figs 6b,c) the pictures show some changes when compared with the previous situation of one cylinder. First, a new resonance appears at the frequency  $k_5 = 4.1$ . This resonance has only two maxima, and so it can be identified as due to movement of the cylinders back and forth in the acoustic field. At this frequency, the two cylinders behave like a single scattering object, and the back and forth movement is linked to the high amplitude oscillations in the area between the cylinders (see Fig 4b). The appearance of new resonances for two shells in an unbounded fluid has been also predicted by Lethullier *et al* (1998).

A second difference between the cases of scattering by one and two cylinders is a wider resonance  $k_2$  for two cylinders. The resonance seems to be split into several new resonances, which are so close that they can not be separated in the picture.

Figs. 6b and 6c, corresponding to the first and second cylinder, for the scattering by two cylinders also have significant differences. First, at the frequency of the lowest resonance both cylinders experience oscillations of maximum amplitude in the direction of the other cylinder, which agrees with the field structure shown in Fig. 4b. Second, the highest resonance  $k_4$  nearly disappears in the picture for the second cylinder. This fact may be explained by the complex interaction between the two resonating cylinders and the waveguide boundaries. Third, the resonance  $k_1$  becomes very indistinct due to



significant changes in the field structure in the surrounding fluid caused by the oscillations of the first cylinder.

### **9.7 Conclusions.**

Modelling has been carried out for scattering by one and by two homogeneous cylinders in a waveguide with a pressure release top surface and a rigid bottom.

Amplitude-frequency and phase-frequency characteristics are obtained for amplitudes of waveguide modes in the reflected and transmitted fields. Sharp increases of modal amplitudes and jumps in their phases are observed near critical frequencies of the waveguide modes and near resonance frequencies of the waveguide system. The amplitudes of both propagating and non-propagating evanescent higher-order modes are found to be considerably different from zero, thus proving the important role of evanescent modes in the scattering process. Values of resonance frequencies may be determined by maxima and minima on the amplitude – frequency characteristics.

The role of higher order modes can be seen also in the pictures of the spatial distribution of the pressure amplitude in the waveguide. It is shown that at a resonance frequency high-amplitude oscillations exist near the scattering objects, which is caused by evanescent modes. In the far field zone, meanwhile, the acoustic field structure is changed significantly at the resonance compared to the structure at non-resonance frequencies. The mechanism of scattering by two cylinders at the resonance is suggested.

The frequency and angular dependencies of the density distribution of the acoustic sources on the cylinder surfaces are obtained for one and two cylinder configurations of the system. A series of resonances with different spatial structure have been identified within the considered frequency range. It is shown that the resonances are associated with structural resonances of the scattering object as well as with surface elastic waves near the cylinder boundary. It is also demonstrated that the resonances correspond to maxima and minima in the amplitude-frequency characteristics. A resonance split is revealed for both configurations, which in the case of one cylinder is explained by coupling of different modes of the cylinder with each other due to interaction with the waveguide walls.

The numerical modelling of the scattering by one and two homogeneous cylinders shows that higher-order waveguide modes play an important role in determining the structure of the scattered sound field in both near and far field zones. The interdependence between the spatial structure of the scattered field, its modal composition, and oscillations of the scattering objects has been clarified.

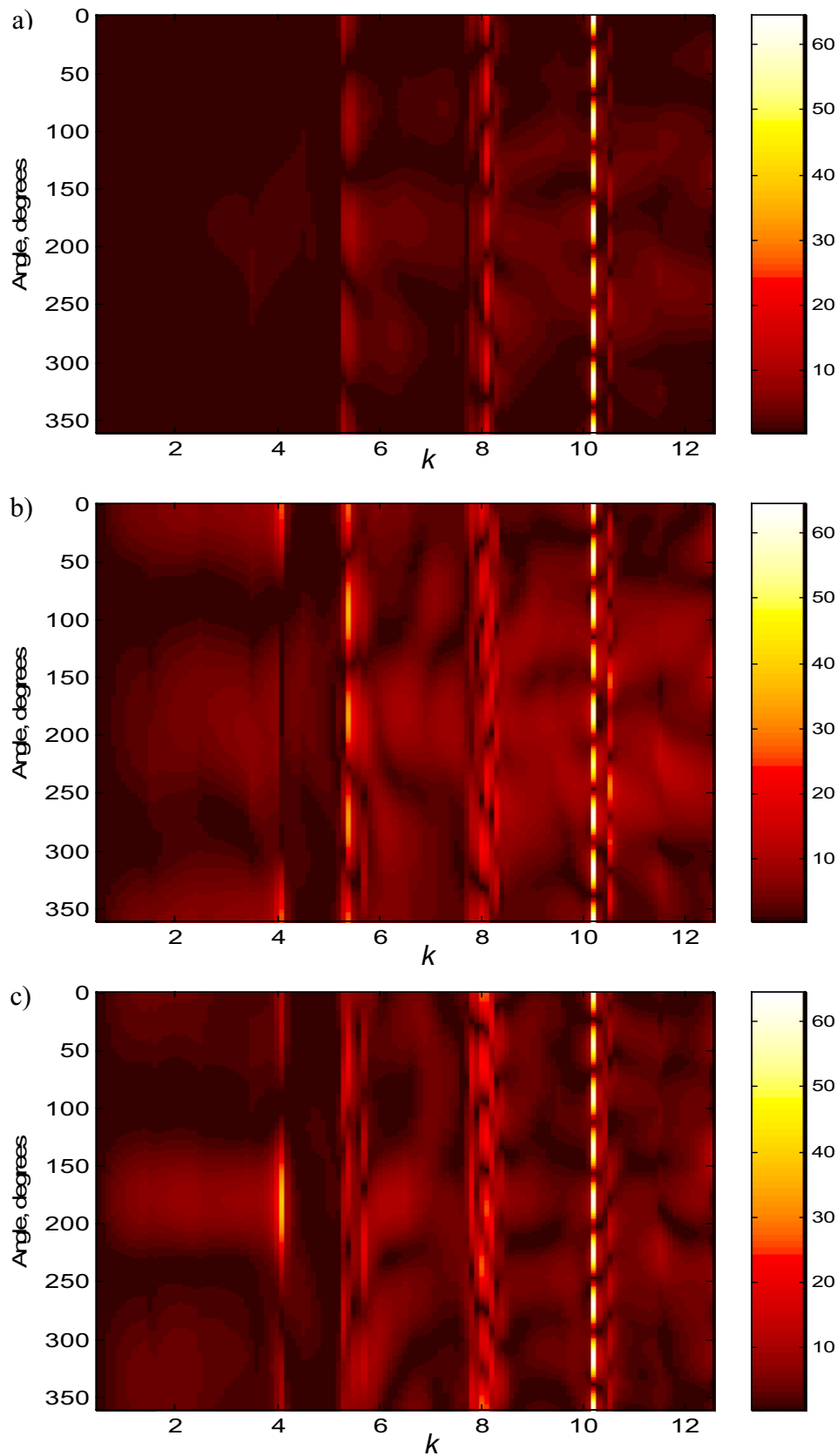


Figure 9. Angle and frequency distribution of the density of acoustic field sources on the surface of the cylinders; a) one cylinder; b) first of the two cylinders; c) second of the two cylinders

## 10 Power Flow of the Scattered Acoustic Wave in a Symmetric Waveguide.

### 10.1 Introduction

Investigation of the spatial distribution of power flow can be useful for the understanding of acoustical and vibrational processes occurring in structures. Time-averaged power flow is best represented by energy streamlines: curves that are tangential to the average sound intensity vector  $\vec{q}$  at any point. Several articles are devoted to the calculation of energy streamlines for various acoustical systems. For example, scattering of a plane acoustic wave by a solid sphere and a spherical shell was considered by Hickling *et al* (1991) and Skelton and Waterhouse (1986). It was shown that acoustic energy could be held in ring-shaped vortices centred near the scattering objects. Scattering in an elastic waveguide by a surface discontinuity (“punch”) was investigated by Glushkov and Glushkova (1997) It was shown that energy vortices can block partially or entirely energy transmission through the cross-section of a waveguide. This section presents the results of calculations of the energy streamlines near a solid cylinder in the plane acoustic waveguide with symmetric boundary conditions: both waveguide walls are considered as perfectly soft pressure release boundaries.

### 10.2 Calculation of Energy Streamlines.

The energy streamlines are defined as the lines to which the acoustic intensity vector is tangential at any point. They can be defined by the following equation:

$$\frac{dy}{dx} = \frac{I_y}{I_x}, \quad (69)$$

where  $I_x, I_y$  are the components of the time-averaged intensity vector,  $\vec{I}$ , which is defined by the well-known expression:

$$\vec{I}(x, y) = \frac{1}{2} \text{Re} [P(x, y) \vec{V}^*(x, y)]. \quad (70)$$

Here  $P(x, y)$  is the amplitude of the total pressure in the fluid, and  $\vec{V}^*(x, y)$  is the complex conjugate of the amplitude of the vibrational velocity vector.

The energy streamlines in the waveguide were drawn as equally spaced contours of the acoustic stream function,  $\Psi(x, y)$ , satisfying the equations:

$$\frac{\partial \Psi(x, y)}{\partial x} = I_y; \quad \frac{\partial \Psi(x, y)}{\partial y} = -I_x, \quad (71)$$

which is equivalent to the definition (69).

The stream function  $\Psi(x, y)$  is calculated as follows:

$$\Psi(x, y) = \int_0^x I_y(x, y) dx. \quad (72)$$

The  $y$ -component,  $I_y$ , of the intensity vector,  $\vec{I}$ , is found as:

$$I_y = \frac{1}{2} \operatorname{Re}[P(x, y)V_y^*(x, y)], \quad (73)$$

where  $P(x, y)$  is determined by the formulas (1) and (68), and the  $y$ -component,  $V_y(x, y)$ , of the velocity vector, is found as:

$$V_y(x, y) = -\frac{i}{\rho\omega} \frac{\partial P(x, y)}{\partial y}. \quad (74)$$

The derivative  $\partial P(x, y)/\partial y$  is determined by differentiating the corresponding formulas.

### 10.3 Parameters of the System.

The parameters used in the calculations are the following (Zinoviev, Belov, 1998):

- Zero pressure on the upper and lower boundaries: ( $\alpha_0 \neq 0$ ,  $\alpha_1 \neq 0$ ,  $\alpha_0 = \beta_0 = 0$ ).
- Parameters of the incident wave:  $A_1 = 1$ ,  $A_n = 0$ ,  $n > 1$ , (Eq. (17))
- Parameters of the fluid:  $\rho = 1000 \text{ kg/m}^3$ ,  $c = 1493 \text{ m/s}$ ;
- Parameters of the cylinder:  $R_0 = D/20$ ,  $\rho_c = 7700 \text{ kg/m}^3$ .

Figs. 10a - 10f show energy streamlines for the cylinder located in the middle of the waveguide, while Figs. 10g,h are for the cylinder displaced in the vertical direction. The power flow is directed from left to right. The coordinates are normalised on the depth  $D$ . The number of the streamlines, shown on top 6 pictures, is 24. The calculations were done for two sets of the longitudinal and transversal velocities:

1. "Rigid" cylinder:  $c_l = 4714 \text{ m/s}$ ,  $c_t = 3223 \text{ m/s}$
2. "Soft" cylinder:  $c_l = 667 \text{ m/s}$ ,  $c_t = 456 \text{ m/s}$ .

### 10.4 Analysis of the Pictures.

The graphs 10a, 10c and 10e correspond to the "rigid" cylinder, while the graphs 10b, 10d and 10f show results for the "soft" cylinder at the same frequency determined by the non-dimensional wavenumber  $k$ .

The top two graphs represent the energy streamlines at low frequency, when only the lowest mode exists in the waveguide. In this case, there is little difference between the two pictures, because the frequency is much lower than any structural resonance of the cylinders including the "soft" one; and both of them behave like "rigid" objects. The acoustic energy is moving from left to right through the cylinders, similar to the way shown for the low-frequency acoustic scattering by a rigid sphere in an unbounded fluid in the paper by Hickling *et al* (1991). This behaviour was explained by rigid-body motion of the object back and forth in the acoustic field. However, the energy streamlines shown in Fig. 10 are not parallel to each other and to the waveguide boundaries in the close vicinity of the cylinder

due to inhomogeneity of the field structure in the waveguide. The distortions of the power flow are caused by higher-order evanescent modes diminishing at larger distances from the cylinder.

The graphs 10c and 10d show the energy streamlines for the wavenumber  $k$  just above the cut-on value for the next symmetric waveguide mode of the order  $n = 3$ . It can be seen clearly, that the power flow pattern has changed abruptly. Instead of the smooth power flow at  $k < 3$ , there are now areas of more and of less intense power flow, revealed by the thickening and rarefying of the energy streamlines. Sharp changes of the power flow inside the sphere were shown by Hickling *et al* (1991) at frequencies near its internal resonances. However, near the cut-on frequency of a waveguide mode the power flow in the whole waveguide changes abruptly. The closed energy streamlines, that is the energy vortices, appear in both the far and the near field because of normal mode interference (Glushkov, Glushkova, 1986). The vortices significantly block part of the waveguide so that the power must flow around the vortices in a way resembling fluid flow over an obstacle. A similar blocking mechanism was described for the scattering by a surface discontinuity (Glushkov, Glushkova, 1986).

A peculiar feature of the graph 10d is the energy vortices, which partially go through the interior of the cylinder. In this case, of the “soft” material the power flow is transmitted through the cylinder by internal oscillations. The two vortices block the central part of the waveguide and produce the pattern, which is repeated throughout all the waveguide. The “rigid” cylinder also produces the energy vortices in the near field, but they are located behind the cylinder and do not go through its interior.

The graphs 10e and 10f correspond to the highest frequency, which coincides with one of the internal resonances of the “soft” cylinder (Belov *et al*, 1994b). The resonance oscillations of the cylinder cause the emergence of the two vortices in the near field in Fig. 10f. These vortices deflect the incoming power flow in the direction of the boundaries, so that together with the cylinder they form a single “scattering object”. Meantime, the “rigid” cylinder still experiences the rigid body back and forth oscillations, transmitting energy in a way revealed in Fig. 10a and 10b.

Calculations of the power flow patterns further to the right show that the pattern repeats itself with little change throughout all the area  $y > 0$ . This is caused by the changes to the amplitudes of the lower order propagating modes occurring near the scattering object.

The existence of the energy vortices going through the scattering object at its internal resonances was shown by Skelton and Waterhouse (1986) by the example of a spherical shell in an unbounded fluid. However, in the waveguide the existence and location of the vortices depend not only on the frequency, but also on other parameters. Figs. 10g and 10h show the energy streamlines near the “soft” cylinder for two different values of its height  $H$  above

the bottom. The number of the streamlines is 40. The graph 10g represents the pattern for the cylinder shifted down from the middle of the waveguide by one radius. It is clearly seen that the near field vortices still exist but the pattern has become asymmetric. When the cylinder height above the bottom is only one quarter of the total depth (Fig.3b), the near field vortices merge with the nearest of the far field vortices. The merging of these vortices forms a single vortex that completely blocks the lower part of the waveguide for the incoming power flow.

The energy vortices are important features in the scattering processes because they may block entirely or partially the cross-section of the waveguide near the resonances of the waveguide or the scattering object. In addition, they may be of importance due to their ability to accumulate acoustic energy. If the incident wave is turned off, the vortices will disintegrate, reradiating the stored acoustic energy and producing the well-known effect of echo in the resonance scattering (Hickling, 1967).

### **10.5 Conclusion.**

Pictures of energy streamlines around a homogeneous cylinder in a waveguide were calculated for different frequencies and different locations of the cylinder in the waveguide. Both resonant and non-resonant cases are considered.

At low frequencies, the energy streamlines are not parallel to each other near the scattering object. The distortions are caused by rigid-body motion of the scattering cylinder back and forth in the acoustic field. There are no closed energy streamlines – energy vortices – in this case.

At the critical frequency of the third waveguide mode, the energy streamline picture changed abruptly. Energy vortices caused by interference of different waveguide modes appear in both near and far field zones, blocking part of the waveguide for incoming acoustic energy.

Energy vortices, which appeared near the scattering cylinder in the case of resonant oscillations of the cylinder, are of major interest. They partially go through the interior of the cylinder, and, thus, involve cylinder oscillations of high amplitude. These vortices are caused by interference of evanescent modes. They represent the elastic and acoustic surface waves near and inside of the cylinder. By blocking part of the waveguide, the vortices effectively increase the scattering cross-section of the cylinder.

This chapter showed that the energy streamlines reveal an important role of higher-order waveguide modes in the scattering process. By interfering with each other, the modes may form the energy vortices, which represent resonance oscillations of the cylinder and of the surrounding fluid.

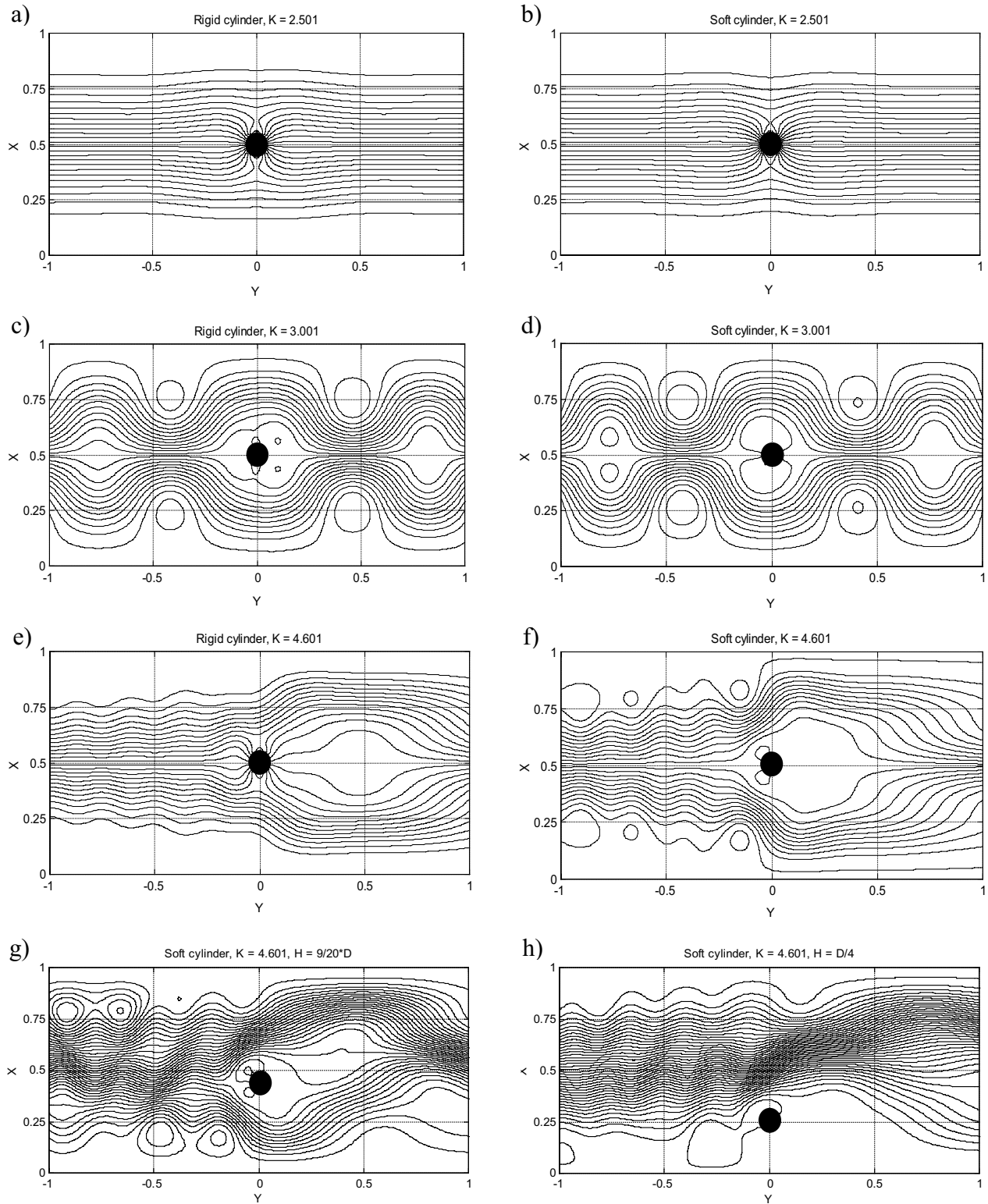


Figure 10. Energy streamlines near the single cylinder. Both waveguide boundaries are perfectly soft. The flow is directed from left to right.

## 11 Oscillations of a Gas Filled Elastic Shell and Reflection of Sound in a Layer of Fluid.

### 11.1 Introduction.

Along with scattering by homogeneous objects like cylinders and spheres, scattering by elastic shells is of major interest due to their closer resemblance to real-world objects. As an object to be investigated, a cylindrical shell shows more complex behaviour due to a more complex internal structure. This chapter presents the analysis of scattering by an air-filled cylindrical shell placed into the plane waveguide described in the previous sections (see Fig. 11)

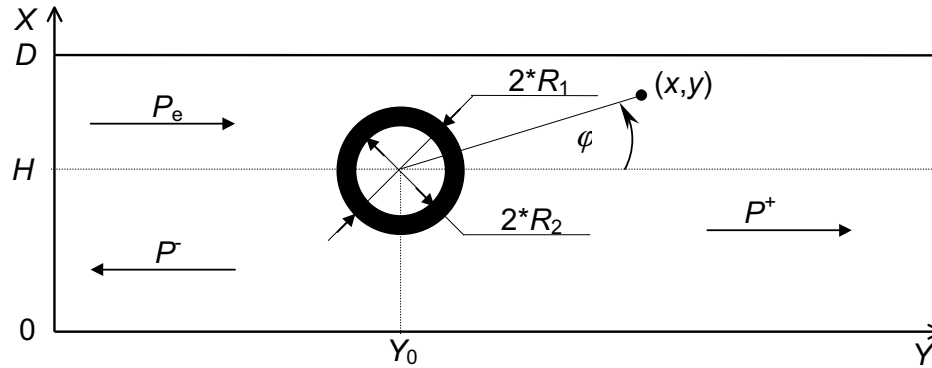


Figure 11. Waveguide with a shell as a scattering object

### 11.2 Differences in the Theoretical Description of Scattering by Homogeneous Cylinders and Shells.

From the considerations shown in section 8 it appears that the theoretical description of scattering by cylindrical objects of different internal structures will be distinct from the description for the homogeneous cylinder only because of different determination of the impedance  $z_m$  on the external boundary described by Eqs. (32), (33), and (64). The impedance of the cylindrical mode of order  $m$  describes the relationship for this mode between the pressure and its radial derivative on the external boundary. A different expression for  $z_m$  is determined by another set of boundary conditions on the internal shell wall, which have the same physical meaning as the conditions (9) – (11).

The impedance for the cylindrical elastic shell is defined as follows (Zinoviev, 1997):

$$z_m = \frac{R_1 \rho (kc)^2}{\mu} \times \frac{\left[ A_m^J im J_m(k_l R_1) + A_m^Y im Y_m(k_l R_1) + B_m^J k_l R_1 J_m'(k_l R_1) + B_m^Y k_l R_1 Y_m'(k_l R_1) \right]}{\left[ i A_m^J \Phi_{1m}^J(k_l R_1) + i A_m^Y \Phi_{1m}^Y(k_l R_1) + B_m^J \Phi_{3m}^J(k_l R_1) + B_m^Y \Phi_{3m}^Y(k_l R_1) \right]} \quad (75)$$



Here the complex amplitudes  $A_m^J, A_m^Y, B_m^J, B_m^Y$  describe elastic waves inside the shell:

$$F(r, \varphi) = \sum_{m=-\infty}^{\infty} (A_m^J J_m(k_t r) + A_m^Y Y_m(k_t r)) \exp(im\varphi), \quad (76.1)$$

$$\Phi(r, \varphi) = \sum_{m=-\infty}^{\infty} (B_m^J J_m(k_t r) + B_m^Y Y_m(k_t r)) \exp(im\varphi). \quad (76.2)$$

The amplitudes  $A_m^J, A_m^Y, B_m^J, B_m^Y$  are defined by the following system of linear equations:

$$\begin{pmatrix} \Phi_{2m}^J(k_t R_1) & \Phi_{2m}^Y(k_t R_1) & -i\Phi_{1m}^J(k_t R_1) & -i\Phi_{1m}^Y(k_t R_1) \\ \Phi_{2m}^J(k_t R_2) & \Phi_{2m}^Y(k_t R_2) & -i\Phi_{1m}^J(k_t R_2) & -i\Phi_{1m}^Y(k_t R_2) \\ imJ_m(k_t R_2) & imY_m(k_t R_2) & R_2 k_t J_m'(k_t R_2) & R_2 k_t Y_m'(k_t R_2) \\ i\Phi_{1m}^J(k_t R_2) & i\Phi_{1m}^Y(k_t R_2) & \Phi_{3m}^J(k_t R_2) & \Phi_{3m}^Y(k_t R_2) \end{pmatrix} \begin{pmatrix} A_m^J \\ A_m^Y \\ B_m^J \\ B_m^Y \end{pmatrix} = \begin{pmatrix} 0 \\ 0 \\ \frac{k_g R_2 J_m'(k_g R_2)}{\rho_g (k_g c_g)^2} \left[ \frac{D}{\pi} \right]^2 \\ -\frac{1}{\mu} R_2^2 J_m(k_g R_2) \left[ \frac{D}{\pi} \right]^2 \end{pmatrix} \quad (77)$$

Here the subscript  $g$  refers to the values in the gas-filled interior of the shell. Auxiliary functions  $\varphi_m(x)$  are defined by the formulas:

$$\Phi_{1m}^J(x) = 2m(xJ_m'(x) - J_m(x)), \quad \Phi_{1m}^Y(x) = 2m(xY_m'(x) - Y_m(x)), \quad (78)$$

$$\Phi_{2m}^J(x) = x^2(J_m(x) + 2J_m''(x)), \quad \Phi_{2m}^Y(x) = x^2(Y_m(x) + 2Y_m''(x)), \quad (79)$$

$$\Phi_{3m}^J(x) = 2x^2(J_m''(x) - \frac{\lambda}{2\mu} J_m(x)), \quad \Phi_{3m}^Y(x) = 2x^2(Y_m''(x) - \frac{\lambda}{2\mu} Y_m(x)). \quad (80)$$

All necessary theoretical calculations, involved in the derivation of the above formulas, are shown in the Appendix C.

### 11.3 Parameters of the System.

The following parameters of the system are used in the numerical calculations of scattering by a cylindrical shell:

- Zero pressure on the upper boundary and zero particle velocity on the bottom, i.e. in terms of the conditions (7) and (8)  $\alpha_0 = \beta_1 = 0, \alpha_1 \neq 0, \beta_0 \neq 0$ .
- Waveguide depth  $D = 80$  m;
- Parameters of the incident wave:  $A_0 = 1, A_n = 0, n > 0$ ;
- Parameters of the fluid:  $\rho = 1000$  kg/m<sup>3</sup>,  $c = 1496.6$  m/s;
- Parameters of the shell:  $R_1 = 8$  m,  $\rho_s = 7900$  m/s,  $\lambda = 1.8 \times 10^{11}$  Pa,  $\mu = 0.7 \times 10^{11}$  Pa;
- Parameters of the gas:  $c_g = 330$  m/s,  $\rho_g = 1.29$  kg/m<sup>3</sup>;

- The wavenumber range: from 0.5 to 32 in steps  $\Delta k = 0.1$ .  $k$  and  $f$  are related as:

$$k = 2fD / c \quad (81)$$

#### 11.4 Analysis.

Figs. 12 and 13 show the result of calculation of the velocity amplitude (left pictures) for comparison with the reflection coefficient (right pictures) for different values of the shell thickness  $d = R_1 - R_2$  and the height  $H$  above the bottom. The reflection coefficient  $R_c$  can be defined as  $S^- / S_e$ . Here  $S_e$  is the total amount of acoustic energy in the incident wave, moving through the vertical cross-section of the waveguide in unit time.  $S^-$  is the amount of energy, reflected in the backward direction from the shell. The mathematical techniques used to obtain the reflection coefficient and the velocity amplitude are shown in Appendix C.

Analysis of the figures 12 and 13 shows:

1. Sharp changes in the spatial distribution of the velocity amplitude in the low frequency range in the vicinity of the critical frequencies of the waveguide coincide with maxima and minima of the reflection coefficient. These maxima and minima are caused by high density of acoustic energy at the critical frequencies.
2. Two narrow resonances of the velocity amplitude at  $k = 16$  and  $k = 25$  in Fig. 12a correspond to minima of the reflection coefficient in Fig. 12b. First of these resonances is a monopole “breathing” mode of the shell, and the second at  $k \cong 25$  is a dipole “translating” mode, occurring without changing the shape of the shell. The former is not the lowest order monopole resonance. The acoustic wavelength in gas at  $k = 16$  is about a quarter of the internal diameter of the shell, which suggests the existence of acoustic standing waves in the interior of the shell. The latter is essentially a resonance of coupled fluid-shell rather than an elastic resonance of the shell itself. It is interesting to notice that the second resonance is split. It consists of two maxima in quadrature, i.e. rotated  $90^\circ$  in space with respect to each other. It demonstrates the coupling between the shell and the waveguide quite clearly. Both the monopole and the dipole oscillations lead to a decrease in the reflected signal, i.e. they increase acoustic energy flow through the shell and its close vicinity, decreasing the scattering cross-section of the shell. Apart from these two resonances, the velocity amplitude has a broad maximum at the front of the shell,  $\varphi = 180^\circ$ . Near zero frequency, the oscillations are nearly monopole due to the proximity of the lowest order breathing resonance of the shell. This leads to the large jumps in the reflection coefficient at low frequencies.

3. When the thickness  $d$  is not zero, but still small (Fig. 12c,d;  $d = 0.01 * R_1$ ), the velocity amplitude distribution shown in Fig. 12c is essentially the same but with two significant differences. First, the dipole resonance has disappeared due to the larger mass of the shell, which is critical for this kind of resonance oscillations. Second, the low frequency maximum of the velocity is shifted from zero frequency to approximately  $k = 5$  due to the influence of the shell elasticity on the monopole resonance. The corresponding maximum in the reflection coefficient is shifted as well (Fig. 12d).

The exact location of the monopole resonance on the reflection coefficient curve (Fig. 12d) can be determined by considering critical frequencies of the waveguide modes. It is clear from the figure that the critical frequencies of the waveguide modes of orders zero and one correspond to maxima in the reflection coefficient. The critical frequency of the second mode corresponds to neither minimum nor maximum, while the critical frequencies of higher modes coincide with the minima in the reflected signal.

Donskoi *et al* (1990) considered the radiation of sound by an air-filled cavity near an oscillating piston. It was shown that the presence of a resonant cavity near a vibrating piston could either amplify the radiation (in the frequency range below resonance) or partially suppress the radiation at frequencies above resonance. Considering this, the curve in Fig. 12d suggests that a lowest order monopole resonance occurs near the critical frequency of the second mode,  $k_2 = 2.5$ . Indeed, at a frequency below  $k_2 = 2.5$ , the lowest waveguide mode radiated by the shell is in phase with the incident field, which consists of only the lowest order mode. These two fields add together coherently in the area behind the shell, thus increasing the transmitted wave and decreasing the reflected wave. At the critical frequencies, however, a significant portion of the acoustic energy, radiated by the shell, transfers to the critical mode, thus decreasing the amplitude of the lowest mode and increasing the reflected signal. In the range above  $k_2 = 2.5$ , where the scattered and the radiated waves are in opposite phase, the mechanism is converse.

According to Donskoi *et al.* (1990), at a point of resonance the field radiated by an oscillating object lags the incident field by  $\pi/2$ . Therefore, the decrease of the amplitude of the lowest order mode does not lead to a significant change in the reflected signal. Thus, at a resonance of the shell a critical frequency of a waveguide mode (in our case  $k_2 = 2.5$ ) is associated with neither a maximum nor a minimum of the reflection coefficient.

4. The sharp decrease of the reflected signal near the monopole resonance A (Fig. 12a,b,c,d) provides an opportunity to suppress the reflection from a submerged elastic object. The

suppression can be done by either selecting the corresponding internal structure of the object or by active excitation of an oscillation, which may transmit the acoustic energy through the object without reflection.

5. The velocity distribution for the thicker shell (Fig. 12e,  $d = 0.05 * R_1$ ) has no noticeable resonances within the frequency range considered apart from very low frequencies. At low frequencies the presence of two maxima indicates dipole vibrations. However, these dipole vibrations can not radiate sound effectively when the wavelength is much larger than the size of the object. Therefore, the reflection is relatively small (Fig. 12f). It can be seen also that the higher cylindrical modes play a bigger role in the shell vibrations at higher frequencies.
6. The velocity pictures for the shell, located in the centre of the waveguide (Fig. 12), are nearly symmetric despite asymmetry in the boundary conditions and the incident wave. However, if the shell is shifted along the vertical direction (Fig. 13) the pictures become substantially asymmetric. This fact proves significant dependence of the shell vibrations in the waveguide on its spatial location.
7. When the distance  $H$  between the bottom and the centre of the shell is a quarter of the waveguide depth  $D$  (Fig. 13a,b), the velocity picture is still nearly symmetric. However, due to the interaction with the rigid bottom, the velocity amplitude distribution shows maxima in the lower half of the shell ( $180^\circ \leq \varphi \leq 360^\circ$ ). These resonances cause indistinct maxima in the reflected signal, but they mutually cancel their contribution to the scattered field in the frequency ranges where they overlap each other.
8. The velocity distribution is much more asymmetric when the shell is located close to the bottom. At the very low frequency, however, the shell experiences only translating oscillations in the horizontal direction (vertical motion is prohibited by the boundary conditions on the bottom). The picture shows two quite strong maxima in the lower part of the shell at the frequencies near  $k = 10$  and 28, which correspond to maxima in the reflection coefficient. These resonances seem to be associated with resonance oscillations of the surrounding fluid between the lower boundary of the shell and the waveguide bottom. The ratio  $(H - R_1)/\lambda$ , where  $\lambda$  is the acoustic wavelength, is close to  $1/4$  at  $k = 10$ , and to  $2/3$  at  $k = 28$ .
9. If the shell is located close to the upper pressure release boundary (Fig. 13e,f), the reflection is very small due to the spatial structure of the incident wave. The velocity distribution has only a broad weak maximum at the lowest point of the shell, which exists throughout all the frequency range considered. However, at the very low frequency the shell experiences

relatively strong translating motion. Opposite to the case when the shell is near the bottom, it moves in vertical rather than horizontal direction due to the pressure release boundary conditions on the surface.

### **11.5 Conclusions.**

This chapter presented the analysis of the velocity distribution on the surface of a scattering gas-filled cylindrical shell. The angular and frequency dependence of the velocity distribution was compared with the frequency dependence of the reflection coefficient. Calculations were carried out for different values of the shell thickness and of the shell location in the waveguide. Different types of resonance oscillations of the shell were identified.

The velocity amplitude experiences sharp changes near the critical frequencies of the waveguide modes. The frequencies of such changes coincide with maxima and minima of the reflection coefficient. These maxima and minima appear due to high density of the acoustic energy near the critical frequencies. Their type (maximum or minimum) depends on the correlations between their frequencies and the frequencies of one of the shell resonances.

For the thin shell two lower resonances of the shell interior, “breathing” and “translating” modes, were revealed. These resonances are correlated with a sharp decrease in the reflected signal, suggesting an opportunity to control the reflection from a submerged elastic target.

When the shell is located close to the waveguide bottom, there are strong velocity maxima in the lowest part of the shell, corresponding to maxima in reflection coefficient. It was suggested, that the resonances are caused by multiple reflections of the sound wave from the bottom and from the shell.

The pictures analysed in this chapter show that the oscillations of a shell as well as its reflection properties depend strongly on the shell thickness and its location in the waveguide. Depending on these parameters and on the frequency of the incident wave, different kinds of resonant oscillations may be excited in the system waveguide/shell. It is shown that the resonances change abruptly the amount of acoustic energy reflected from the shell.

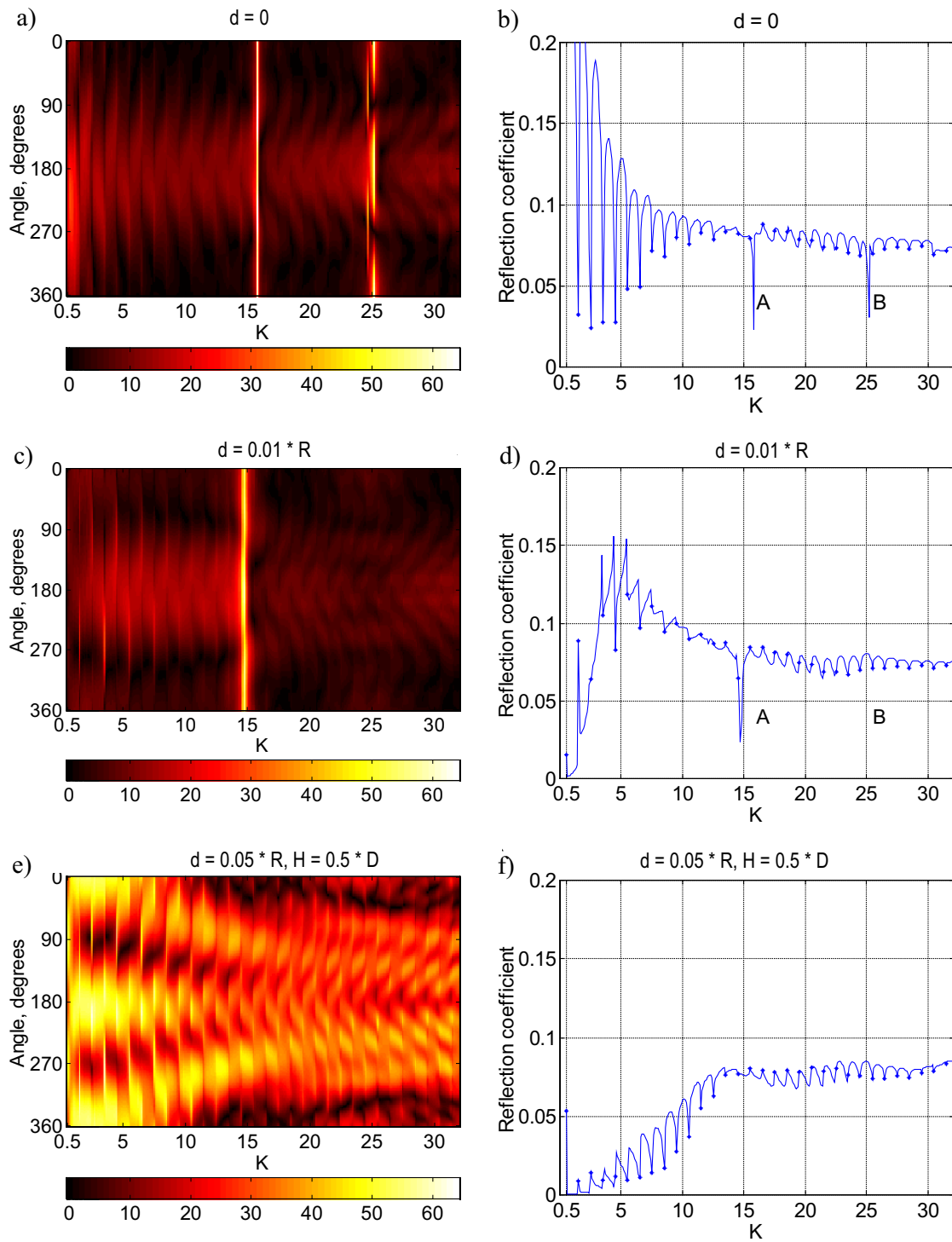


Figure 12. Results of calculations for shells with different thicknesses  $d$  located in the centre of the waveguide. Left: Dependence on the frequency of the angular distribution of the velocity amplitude on the outer shell surface. Light areas correspond to high amplitude and dark areas correspond to low amplitude. Right: the frequency dependence of the reflection coefficient. Dots reveal the critical frequencies of the waveguide  $k = n + 1/2$ .

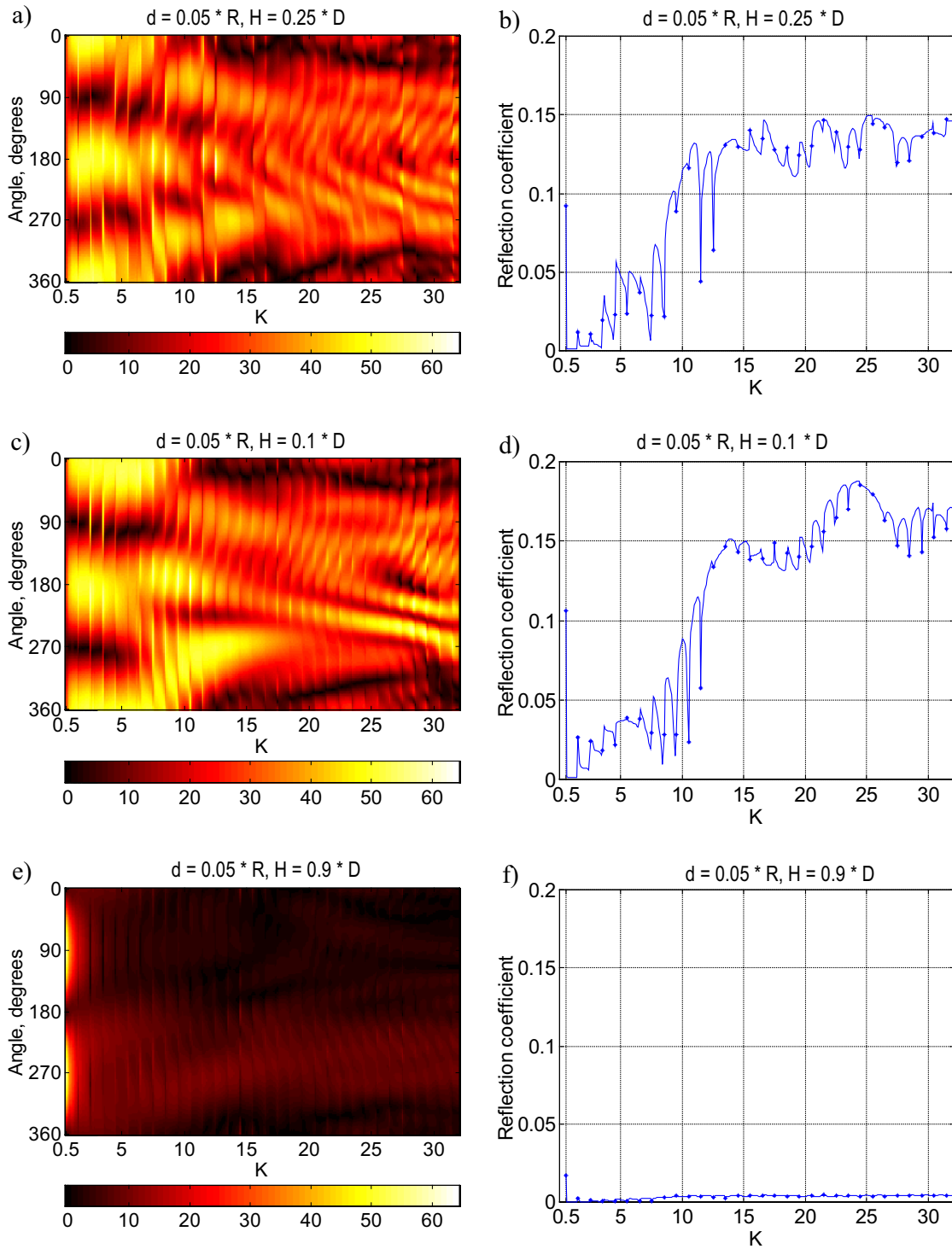


Figure 13. Results of calculations for shells with the same thickness  $d = 0.05 * R_1$  and different location in the waveguide. Left: dependence on the frequency of the angular distribution of the amplitude of velocity on the outer shell surface. Light areas correspond to high amplitude and dark areas correspond to low amplitude. Right: the frequency dependence of the reflection coefficient. Dots reveal the critical frequencies of the waveguide  $k = n + 1/2$ .